

Total Energy as a Function of Lattice Parameter for Copper
Using the Self-Consistent APW Method

by

Edward Clark Snow

A DISSERTATION PRESENTED TO THE GRADUATE COUNCIL OF
THE UNIVERSITY OF FLORIDA IN PARTIAL
FULFILLMENT OF THE REQUIREMENTS FOR THE DEGREE OF
DOCTOR OF PHILOSOPHY

UNIVERSITY OF FLORIDA
1973

ACKNOWLEDGMENTS

I would like to thank Professors J. C. Slater and J. W. D. Connolly and the other members of the Quantum Theory Project at the University of Florida for helpful comments concerning this work. A special thanks is due Dr. John H. Wood for his many helpful suggestions, his constructive criticism of the manuscript, and his continuous understanding and encouragement. The continued interest and assistance of F. W. Schonfeld is also appreciated.

I would also like to express my appreciation for the help and consideration afforded me by the many members of the Central Computer Facility at the Los Alamos Scientific Laboratory. The support of the U. S. Atomic Energy Commission is also gratefully acknowledged.

TABLE OF CONTENTS

	Page
ACKNOWLEDGMENTS	ii
LIST OF TABLES	v
LIST OF FIGURES	vi
ABSTRACT	viii
CHAPTER I INTRODUCTION	1
1.1. Purpose	1
1.2. Outline of Calculation	4
CHAPTER II METHODS OF CALCULATION	6
2.1. The Self-Consistent APW Method	6
2.2. The $X\alpha$ Exchange Approximation	14
2.3. Potentials	19
2.4. Total Energy and Cohesive Energy	24
2.5. Pressure and Compressibility	27
CHAPTER III RESULTS OF THE CALCULATION FOR COPPER	30
3.1. Determining α of the $X\alpha$ Method	30
3.2. Total Energy and Cohesive Energy Results	31
3.3. Pressure and Compressibility	41
3.4. Energy Bands and Density of States	47
CHAPTER IV CONCLUSIONS	71
APPENDIX A METHODS OF IMPROVING THE ACCURACY OF THE LOGARITHMIC DERIVATIVES USED IN AN APW CALCULATION	75
A.1. Introduction	75
A.2. Starting Values	76
A.3. Evaluation of the Derivatives at R_g	79
A.4. Effects of the Choice of Radial Mesh	81

	Page
APPENDIX B	
TOTAL ENERGY CALCULATIONS USED TO EVALUATE THE "FROZEN CORE" MODEL	93
APPENDIX C	
THE ENERGY BANDS, DENSITY OF STATES, TOTAL ENERGY, AND COHESIVE ENERGY OF COPPER AS A FUNCTION OF α	97
C.1. The Energy Bands and Density of States	97
C.2. Total Energy and Cohesive Energy as a Function of α for Copper ($A=A_0$)	117
LIST OF REFERENCES	126
BIOGRAPHICAL SKETCH	129

LIST OF TABLES

Table	Page
3.1. The pressure, potential energy, kinetic energy, and total energy for four self-consistent APW calculations on copper, with different values of α	32
3.2. Total energy for six values of the lattice parameter for copper ($\alpha = 0.7225$)	38
3.3. The pressure for five values of the cell volume of FCC copper, evaluated using the virial theorem (vt) and the slope of the energy vs. volume curve at V_0 (E vs. V).....	44
3.4. Energy differences for states that indicate positions and widths of the sp-band and d-band (Ry)	69
A.1. The logarithmic derivatives U'_ℓ/U_ℓ , evaluated at $R_S = 2.5$, for a $-2Z/r$ potential, with $Z = 26$, on a logarithmic mesh	83
A.2. The relative error in the logarithmic derivatives for four linear radial meshes, with $R_S = 2.5$ a.u., $Z = 26$ a.u., and $E = 0.10$ Ry, for a $-2Z/r$ test potential	91
A.3. Relative error in the core state eigenvalues for four linear meshes, with $R_S = 2.5$ a.u., $Z = 26$ a.u., and a $-2Z/r$ test potential	92
B.1. Total energies for self-consistent atomic and crystal calculations on copper with $\alpha = 0.7225$, for two core configurations	95
C.1. Energy differences for states that indicate positions and widths of sp-band and d-band (Ry)	115
C.2. Total energy and cohesive energy as a function of α for copper ($A=A_0$)	118

LIST OF FIGURES

Figure	Page
2.1. The first Brillouin zone associated with the FCC structure, showing the 1/48 of the zone in which solutions for the \underline{k} vectors are considered	9
2.2. Qualitative graph of the ground state total energy of a crystal as a function of the lattice parameter.....	18
3.1. Pressure vs. α of the $X\alpha$ method for copper	34
3.2. The total energy vs. α of the $X\alpha$ method for copper.....	36
3.3. The total energy as a function of lattice parameter for copper ($\alpha = 0.7225$)	40
3.4. The total energy as a function of volume for copper, near the minimum. ($\alpha = 0.7225$).	43
3.5. Pressure as a function of volume.....	46
3.6. (a & b) Energy bands for FCC copper with $\alpha = 0.7225$ and $A = 6.321$ a.u. (c) Density of states for this calculation..	49
3.7 (a & b) Energy bands for FCC copper with $\alpha = 0.7225$ and $A = 6.574$ a.u. (c) Density of states for this calculation..	53
3.8. (a & b) Energy bands for FCC copper with $\alpha = 0.7225$ and $A = 6.809$ a.u. (c) Density of states for this calculation..	57
3.9. (a & b) Energy bands for FCC copper with $\alpha = 0.7225$ and $A = 7.028$ a.u. (c) Density of states for this calculation..	61
3.10. (a & b) Energy bands for FCC copper with $\alpha = 0.7225$ and $A = 7.235$ a.u. (c) Density of states for this calculation..	65
A.1. The $\ell = 0$ logarithmic derivatives for a $-2Z/r$ potential as a function of the logarithmic mesh.....	86
A.2. The $\ell = 1$ logarithmic derivatives for a $-2Z/r$ potential as a function of the logarithmic mesh.....	88

Figure	Page
A.3. The $\ell = 2$ logarithmic derivatives for a $-2Z/r$ potential as a function of the logarithmic mesh.....	90
C.1. (a & b) Energy bands for FCC copper with $\alpha = 0.700$ and $R_s = 2.407$ a.u. (c) Density of states for this calculation..	99
C.2. (a & b) Energy bands for FCC copper with $\alpha = 0.70635$ and $R_s = 2.407$ a.u. (c) Density of states for this calculation..	103
C.3. (a & b) Energy bands for FCC copper with $\alpha = 0.720$ and $R_s = 2.407$ a.u. (c) Density of states for this calculation..	107
C.4. (a & b) Energy bands for FCC copper with $\alpha = 0.770$ and $R_s = 2.407$ a.u. (c) Density of states for this calculation..	111
C.5. Total energy as a function of the parameter α , for metallic copper ($A = A_0$)	120
C.6. Total energy as a function of the parameter α , for atomic copper	122
C.7. The cohesive energy of copper as a function of the parameter α of the $X\alpha$ method ($A = A_0$)	124

Abstract of Dissertation Presented to the
Graduate Council of the University of Florida in Partial Fulfillment
of the Requirements for the Degree of Doctor of Philosophy

TOTAL ENERGY AS A FUNCTION OF LATTICE PARAMETER FOR
COPPER USING THE SELF-CONSISTENT APW METHOD

By
Edward Clark Snow

August, 1973

Chairman: J. W. D. Connolly
Major Department: Physics

The $X\alpha$ exchange approximation is used in self-consistent APW calculations on metallic copper. The α used in the $X\alpha$ method ($\alpha = 0.7225$) was chosen to yield zero pressure at the experimentally determined lattice spacing. Self-consistent APW calculations were carried out for six different lattice parameters, using this value of α . The total energy as a function of lattice parameter resulting from these calculations was used to determine pressure as a function of lattice parameter, cohesive energy, and compressibility. The cohesive energy for the calculation using the experimental lattice parameter and $\alpha = 0.7225$ was found to be 0.286 Ry, which is within 11% of the experimental value of 0.257 Ry. The compressibility was calculated from two sets of calculated pressures as a function of lattice parameter and was

found to agree with the experimental value to within 7% in one case and to within 4% in the other.

CHAPTER I

INTRODUCTION

1.1 Purpose

With the development of large fast computers, many methods of determining the electronic structure of solids have become practical. These methods employ various approximations to simplify the calculations, with a minimum loss of accuracy. Within two of these, namely the nonrelativistic and electrostatic approximations, the Hamiltonian operator for a crystal can be written as

$$H_{\text{op}} = -\sum_{\mu} \frac{\hbar^2}{2M_{\mu}} \nabla_{\mu}^2 - \sum_j \frac{\hbar^2}{2m_o} \nabla_j^2 + V(X_{\mu}, x_j) \quad (1.1)$$

where the first term is the kinetic energy term associated with the motion of the nuclei of masses M_{μ} , the second is the kinetic energy term associated with the motion of the electrons of masses m_o , and the last term is the potential energy term, which includes nuclear-nuclear, electron-nuclear, and electron-electron coulomb interactions, plus the electron-electron exchange interactions. In the Born-Oppenheimer approximation, which is based on the assumption that since $M_{\mu} \gg m_o$, the electronic motion can be treated separately

from the nuclear motion, the first term in Eq. (1.1) vanishes, yielding the electron Hamiltonian as

$$H_{\text{op}} \simeq -\sum_j \frac{\hbar^2}{2m_0} \nabla_j^2 + V(X_\mu, x_j). \quad (1.2)$$

The Schrödinger equation for the system is then given as

$$\left[-\sum_j \frac{\hbar^2}{2m_0} \nabla_j^2 + V(X_\mu, x_j) \right] U(X_\mu, x_j) = E(X_\mu) U(X_\mu, x_j) \quad (1.3)$$

where the energy, $E(X_\mu)$, depends on the positions of the nuclei, X_μ , only as a parameter. This is the total energy that is considered in this calculation as a function of lattice parameter.

Recently, considerable effort has been concentrated on developing an approximation to the electronic exchange interaction term in the crystal Hamiltonian that can be used to determine the electronic states of a solid with reasonable accuracy. The purpose of this dissertation is to apply one such exchange approximation to the evaluation of the energy-bands of metallic copper, using the self-consistent APW method, and to determine the total energy as a function of lattice parameter. These results can then be used to obtain such quantities as pressure as a function of lattice parameter, compressibility and cohesive energy.

The exchange approximation that is used in this work is known as the $X\alpha$ approximation. This method began with the so-called $p^{\frac{1}{3}}$ approximation, originally proposed by Slater.¹ Later when Gaspar² and Kohn and Sham,³ using a slightly different approach, derived a

$\rho^{\frac{1}{3}}$ exchange approximation that differed from that of Slater's original result by a constant multiplier of $2/3$, it was indicated that a reasonable exchange approximation could be obtained by multiplying the Slater exchange by an adjustable parameter, α , thus the $X\alpha$ method. There have been many other exchange approximations suggested, both local and non-local in nature. However, the use of several of these on the energy-bands of copper by Boring and Snow⁴ have failed to produce results that are significantly better than those obtained using the less complicated $X\alpha$ method.

This study was conducted on copper for several reasons, the first of which is that the author^{5, 6} has done considerable work on the energy-bands of copper in the past. There is also a large number of other calculations on copper available in the literature with which to compare and experimental results are readily available. The author⁷ has also presented calculations on silver, but silver, having a greater atomic number than copper, should be affected more by relativistic effects which are not considered in the present work. Aluminum might have also been considered, since aluminum energy-band calculations had also been presented by the author,⁸ but aluminum has been studied in great detail by Ross and Johnson.⁹ Another reason for selecting copper over aluminum is the large number of d-like electrons in a nearly filled d-band. It has been observed in past work that these d-bands are very sensitive to small changes in the

exchange potential used in the calculation, whereas the broad sp-band as found in aluminum remains virtually unaffected. This, of course, makes copper a good test case when considering various exchange approximations and their effects on the resulting energy-bands.

The method of calculation is described in detail in Chapter II with an outline of the procedure given in the next section. Chapter III is devoted to the results of the calculations as applied to copper and the comparison of these results with previously calculated and experimental results. The discussions and conclusions are given in Chapter IV.

1.2 Outline of Calculation

These calculations employ the augmented plane wave (APW) method¹⁰ for determining the energy-bands. In this method the "muffin tin" approximation to the potential is used, which has been found to give very good results in energy-band calculations of this type. In the "muffin tin" approximation the electronic potential energy function is considered to be spherically symmetric within non-overlapping spheres centered at each lattice site and constant in the region between spheres. DeCicco¹¹ has found that the "non-muffin tin" terms should have very little effect in an energy-band calculation of an FCC metal like copper, and these terms are not considered in these calculations.

The self-consistent calculation is started with a potential that is generated by the superposition of atomic potentials centered at each lattice site. This potential is then used in the APW calculation to determine the energy-bands and corresponding charge density of the filled Bloch states. The energies and charge densities of the core states are determined in a manner similar to that used in the Herman and Skillman¹² atomic calculations with the appropriate boundary conditions. The total charge density, core plus energy-band, is then used to generate a new potential to be used in the next iteration of the self-consistent process. This iterative process is continued until there is no significant difference between the one-electron energies obtained in two successive iterations.

This self-consistent method is used for calculations at various lattice parameters so that the total energy as a function of lattice parameter can be determined. Pressure, compressibility and cohesive energy can then be determined and compared to experimental results and the results of previous calculations.

These calculations are all done for an appropriate value of the parameter α of the $X\alpha$ method, the choice of which will be discussed in detail along with the rest of the method in Chapter II.

CHAPTER II

METHODS OF CALCULATION

2.1 The Self-Consistent APW Method

Since the introduction of the augmented plane wave (APW) method by Slater¹⁰ in 1937, it has been used for a large number of calculations on solids with very good results in most cases. Loucks¹³ and more recently, Mattheiss, Wood, and Switendick¹⁴ have presented articles that not only describe in detail Slater's original presentation, but also cover the use of group theory and self-consistency. To present the APW method in detail here would be to rewrite their articles. Since this would be a waste of time and space, what follows is a short review of the method that parallels the article by Mattheiss et al.¹⁴

The method is designed to solve the on-electron Schrödinger equation in a periodic potential $V(\underline{r})$ such as

$$V(\underline{r} + \underline{T}_n) = V(\underline{r}) \quad (2.1)$$

where \underline{T}_n is any lattice vector of the crystal structure. The one-electron equation is then given by

$$H \psi(\underline{r}; \underline{k}) \equiv \left[-\nabla^2 + V(\underline{r}) \right] \psi(\underline{r}; \underline{k}) = E(\underline{k}) \psi(\underline{r}; \underline{k}) \quad (2.2)$$

with the energy $E(\underline{k})$ in Rydbergs and the distances expressed in Bohr radii. In the original APW method as well as in most variations of it

used recently, the potential function $V(\underline{r})$ is usually considered to be of the "muffin tin" form. Although this is not a very strong restriction on calculations in metals such as copper, DeCicco¹¹ has indicated how one can evaluate the corrections associated with the "non-muffin tin" terms of the potential. The methods used to construct the potentials used in the present work are discussed in detail in Sec. 2.3.

The wave functions that are solutions to Eq. (2.2) are Bloch type functions¹⁵ and can be written

$$\psi(\underline{r};\underline{k}) = \exp(i\underline{k} \cdot \underline{r}) U(\underline{r};\underline{k}) \quad (2.3)$$

where $U(\underline{r};\underline{k})$ is a periodic function of the lattice such that

$$U(\underline{r} + \underline{T}_n; \underline{k}) = U(\underline{r}; \underline{k}) \quad (2.4)$$

with \underline{T}_n equal to any lattice vector. It should be noted that the energy as well as the wave function are dependent on the selection of \underline{k} , the wave vector. This vector corresponds to a vector in the reciprocal space associated with the crystal structure. To solve the energy-band problem, values of the wave vector \underline{k} must be selected, for which the solutions to Eq. (2.2) are to be determined. Due to the translational symmetry of the reciprocal space, one needs only to consider vectors in the first Brillouin zone.¹⁵ Also due to the symmetry of the first Brillouin zone itself, one needs to determine solutions for only those wave vectors within 1/48 of the zone (in our face-centered cubic problem), as shown in Fig. 1. Of course, this still represents an infinite

Figure 2. 1. The first Brillouin zone associated with the FCC structure, showing the $1/43$ of the zone in which solutions for the \mathbf{k} vectors are considered.

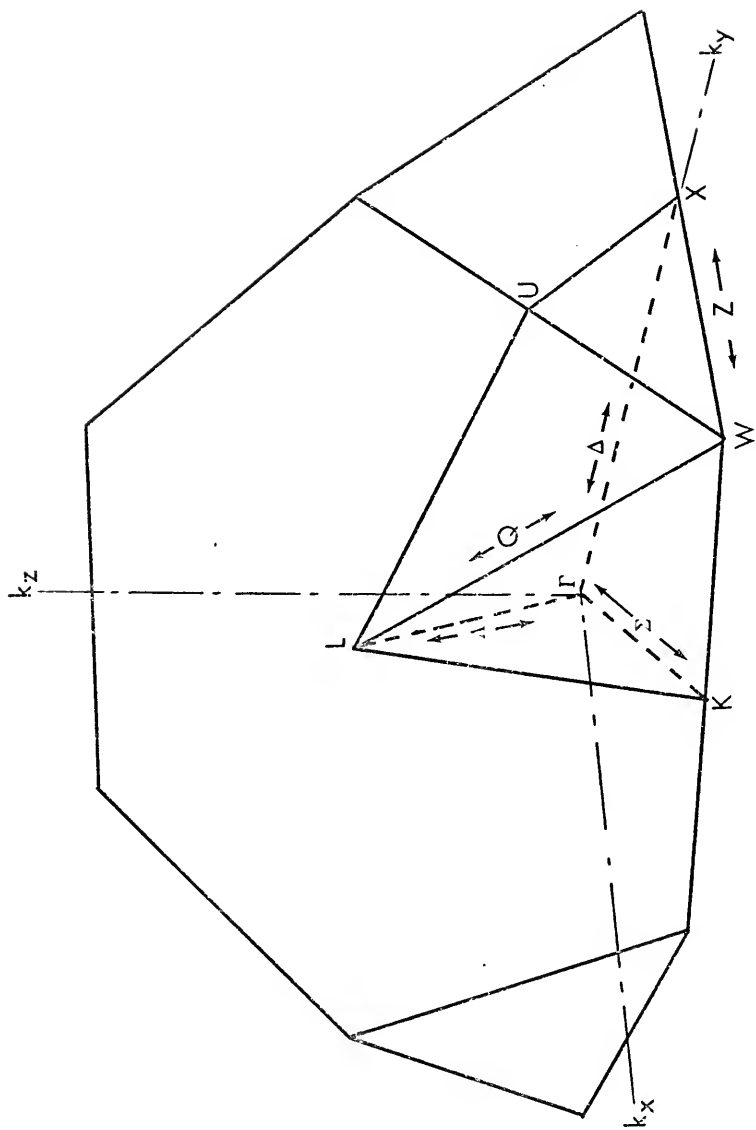


Figure 2.1 BRILLOUIN ZONE - FCC

number of unique vectors to solve for. When one attempts to solve an actual problem, the first Brillouin zone is divided into a grid of equally spaced points, the spacing depending on the accuracy required in determining the resulting energy-bands. Again, one need only consider those points and associated vectors that are contained in 1/48 of the zone. Some of these points and their labels are also indicated in Fig. 1. The one-electron Schrödinger equation, Eq. (2.2), is then solved for the eigenvalues and wave functions at each of these points. The resulting charge density associated with each vector \underline{k} is then weighted by the fractional part of an electron that can be accommodated by this state. This weight is determined to be

$$W(\underline{k}) = 2 \cdot f_{\underline{k}} \cdot 48 \quad (2.5)$$

where $f_{\underline{k}}$ is the fraction of the total volume of the first Brillouin zone associated with that point. This is then multiplied by 48, since only points in 1/48 of the zone are considered in the actual calculations and the factor 2 is introduced to accommodate the two possible spin states. It should be noted that if the solution for the lowest energy is found for each of the points in the first Brillouin zone, this represents a collection of electronic energy values, called the first band, that will accommodate two electrons of opposite spins. If the potential has a spin dependent term, then there are different solutions for each spin state,¹⁶ and the factor 2 is left out of the equation for the weight, Eq. (2.5).

In the APW method, solutions to the one-electron Schrödinger equation are taken to be linear combinations of functions called augmented plane waves (APW's)

$$\psi(\underline{r}; \underline{k}) = \sum_i v(\underline{k}_i) \phi(\underline{r}; \underline{k}_i, E) \quad (2.6)$$

where $\underline{k}_i = \underline{k} + \underline{K}_i$ with \underline{K}_i defined as a reciprocal lattice vector, and the v 's are variational coefficients. By application of the variational method, an APW secular equation can be obtained, the roots of which are the approximate energy eigenvalues of the state being considered; solution of this secular equation also yields the eigenvectors $v(\underline{k}_i)$.

Each APW is defined as a plane wave in the region between "muffin tin" spheres, called APW spheres,

$$\phi(\underline{r}; \underline{k}_i, E) = \exp(i \underline{k}_i \cdot \underline{r}) \quad (2.7)$$

and is expanded in terms of spherical harmonics inside the APW spheres. Within the sphere centered at \underline{r}_n ,

$$\phi(\underline{r}; \underline{k}_i, E) = \sum_{\ell=0}^{\infty} \sum_{m=-\ell}^{\ell} A_{\ell m}(\underline{k}_i) U_{\ell}(|\underline{r} - \underline{r}_n|; E) P_{\ell}^m(\cos \theta) \exp(i m \varphi) \quad (2.8)$$

where the coefficients $A_{\ell m}(\underline{k}_i)$ are chosen so that the function is continuous in value at the APW sphere radius R_n . $U_{\ell}(|\underline{r} - \underline{r}_n|; E)$ in Eq. (2.8) are the solutions to the radial Schrödinger equation

$$-\frac{1}{r^2} \frac{d}{dr} \left(r^2 \frac{dU}{dr} \right) + \left(\frac{\ell(\ell+1)}{r^2} + V_n \right) U_{\ell} = E U_{\ell} \quad (2.9)$$

where V_n is the spherically symmetric part of the potential centered about \underline{r}_n .

Solving for the coefficients $A_{\ell m}(\underline{k}_i)$ by matching the value of Eq. (2.7) and Eq. (2.8) at the sphere radius R_n , yields the APW within the sphere centered at \underline{r}_n

$$\begin{aligned} \Phi(\underline{r}; \underline{k}_i, E) = \exp(i \underline{k}_i \cdot \underline{r}_n) \sum_{\ell=0}^{\infty} \sum_{m=-\ell}^{\ell} (2\ell+1) i^{\ell} \frac{j_{\ell}(k_i R_n)}{U_{\ell}(R_n; E)} U_{\ell}(|\underline{r} - \underline{r}_n|; E) \\ \times \frac{(\ell - |m|)!}{(\ell + |m|)!} P_{\ell}^{|m|}(\cos \theta) P_{\ell}^{|m|}(\cos \theta_i) \exp[i m (\Phi - \Phi_i)] \end{aligned} \quad (2.10)$$

where θ_i and Φ_i are the spherical coordinates of \underline{k}_i with respect to a coordinate system centered about \underline{r}_n .

The variational method, when applied to Eq. (2.2), yields a set of N simultaneous equations

$$\sum_{j=1}^N (H-E)_{ij} v(k_j) = 0; \quad i = 1, 2, \dots, N \quad (2.11)$$

Where N is the number of APW's in the expansion of the wave function and $(H-E)_{ij}$ is the matrix element between APW's

$$(H-E)_{ij} \equiv \langle \Phi(\underline{r}; \underline{k}_i, E) | H-E | \Phi(\underline{r}; \underline{k}_j, E) \rangle. \quad (2.12)$$

Note that E occurs both explicitly and implicitly. In order to solve for the eigenvalues, one must locate the energy E for which the determinant of the matrix of $(H-E)_{ij}$ vanishes. This is usually done by evaluating this determinant for a set of evenly spaced values of E in the range of interest, and locating the E's that correspond to the zeros of the determinant by linear interpolation. The determinant for this energy is then evaluated, and used to locate the eigenvalue more

accurately. This iterative procedure is continued until the energy is located as accurately as desired for the calculation being considered.

Group theory is used to simplify the problem somewhat. If the irreducible representations of the point group of the wave vector \underline{k} are determined, they can be used to greatly reduce the dimensions of the determinant to be evaluated, thus speeding up the entire process. These irreducible representations also yield information about the transformation properties of the states associated with the wave vector \underline{k} . The application of group theory to the APW method is discussed in detail in the work of Mattheiss, Wood, and Switendick,¹⁴ and will not be discussed further here.

Once an eigenvalue is determined to the desired accuracy, it is used in Eq. (2.11) to evaluate the eigenvector $v(\underline{k}_i)$. With this information, the spherically averaged charge density for the state corresponding to \underline{k} and E can be determined and weighted according to Eq. (2.5).

The eigenvalues and corresponding wave functions for the core states, defined as the lower energy atomic-like electronic states that can not be determined by the APW method, are determined in a manner similar to that used by Herman and Skillman¹² in their atomic calculations. The eigenvalues are located by requiring that the logarithmic derivatives of the radial wave function from outward and inward integration of the radial Schrödinger equation, Eq. (2.9), match at the classical turning point. The boundary conditions placed

on the wave functions were

$$U_{\ell}'(R_n;E) = 0; \quad \ell = 0, 2, 4, \dots \quad (2.13)$$

and

$$U_{\ell}(R_n;E) = 0; \quad \ell = 1, 3, 5, \dots \quad (2.14)$$

where the prime indicates the derivative of the function and both the function and its derivative are evaluated at the APW sphere boundary. These boundary conditions were used to preserve the translational symmetry and at the same time resulted in continuity of the value and slope of the wave function in the direction of nearest neighbors.

The total electronic charge density is then determined as the sum of the weighted charge densities associated with the filled band states and the charge densities of the core states. This charge density, along with that associated with the nuclei, is then used to evaluate a new potential and the next step of the self-consistent procedure is started. This iterative process is continued until the difference in energy associated with any state, band or core, obtained in two successive iterations is as small as desired.

2.2 The X_{α} Exchange Approximation

In the one-electron Schrödinger equation used in this calculation, Eq. (2.2), the spherically symmetric potential can be written

$$V(r) = V_c(r) + V_x(r) \quad (2.15)$$

where $V_c(r)$ is the one-electron potential due to the coulomb interaction of the electron under consideration with all electronic charges (including

itself) and $V_x(r)$ is the exchange term. If the Hartree-Fock form of the exchange potential is used, a different exchange potential is required for each electron; construction of these potentials involves sums and integrals over all the other wave functions. In a solid calculation, with the large number of functions involved, a calculation using this type of exchange potential becomes extremely difficult.

What is needed is an approximation to the exchange potential which is the same for all electrons and easier to construct. Just such a potential, based on the average exchange potential in the free electron gas, was given by Slater¹ as

$$V_{xs}(\underline{r}) = -6 \left[\frac{3}{8\pi} \cdot \rho(\underline{r}) \right]^{\frac{1}{3}} \quad (2.16)$$

where $\rho(\underline{r})$ is the total electronic charge density at the point \underline{r} . If $\rho(\underline{r})$ is spherically symmetric about the origin, $V_{xs}(\underline{r})$ is also spherically symmetric and if we define a radial charge density $\rho(r)$ by

$$\rho(r) = \frac{\rho(r)}{4\pi r^2} \quad (2.17)$$

then substituting Eq. (2.17) into (2.16), the Slater exchange potential is given as

$$V_{xs}(r) = -3 \left[\frac{3}{4\pi} \cdot \frac{\rho(r)}{r^2} \right]^{\frac{1}{3}} \quad (2.18)$$

Gaspar² and later Kohn and Sham³ used a variational approach to determine an approximation to the exchange potential of the same form, but found it to be 2/3 as large as the Slater exchange approximation. This indicated that possibly a reasonable approximation to the exchange potential would be what is now called the $X\alpha$ exchange approximation, given by

$$V_{X\alpha}(r) = \alpha V_{XS}(r) = -3\alpha \left[\frac{3}{4\pi^2} \cdot \frac{\rho(r)}{r^2} \right]^{\frac{1}{3}} \quad (2.19)$$

where α ($\alpha = 2/3$ in the Kohn-Sham case) is an adjustable parameter to be selected to fit the problem under consideration. Since then, several calculations have been presented on both atoms and solids using this parametrized one-electron exchange potential, with reasonable success.

There is still the question of the choice of the parameter α for a particular calculation. In a recent paper, Schwarz¹⁷ describes three methods for determining α in atomic calculations. The first was suggested by Lindgren,¹⁸ in which the α is chosen so that the Hartree-Fock total energy, determined from the $X\alpha$ orbitals, is a minimum. This α , called α_{\min} , has been evaluated for several elements by Kmetko¹⁹ and Wood.²⁰ The second method, suggested by Berrondo and Goscinski,²¹ is based on the quantum-mechanical virial theorem and recommends that the α_{vt} should be chosen so that the virial coefficient η , given by

$$\eta = - \langle P.E. \rangle / 2 \langle K.E. \rangle \quad (2.20)$$

where $\langle P.E. \rangle$ and $\langle K.E. \rangle$ are the average potential and kinetic energies, respectively, calculated from the Hartree-Fock expression using $X\alpha$ orbitals, be equal to 1. The third method chooses α , called α_{HF} , so that the statistical total energy, defined for a crystal in Sec. 2.4, of the $X\alpha$ method equals the Hartree-Fock average energy of configuration²²⁻²⁴ for the ground state of the atom. Schwarz has

determined the values of α_{vt} and α_{HF} for the first 41 elements and has found that they differ by less than 0.0008 in every case except hydrogen. Slater and Wood²⁵ have recommended using α_{HF} in a solid calculation. Energy band calculations similar to the one presented here, using values of α given by Schwarz have been done by Averill^{26, 27} and Hattox.²⁸

In the present calculation, α is chosen, that is similar to α_{vt} , such that the virial coefficient equals unity in the crystal at the experimentally determined lattice parameter appropriate for 0°K. This is equivalent to requiring that the minimum of the total energy vs. lattice spacing curve fall at the experimental value of the lattice parameter (A_0) as shown in Fig. 2:2. Since the APW method already requires the lattice parameter as an input parameter, this method of determining α adds no new calculational parameters (either from experiment or from atomic calculations). There are two ways to find this α . One is to determine the movement of the minimum of the total energy vs. lattice spacing curve as a function of α and then to use this information to determine the desired value. This, of course, requires a reasonably large number of self-consistent APW calculations for the various values of α and the lattice parameter.

The other way involves the virial theorem, given by

$$\langle K. E. \rangle = - 1/2 \left[\sum_i x_i F_i \right]_{av} \quad (2.21)$$

where $\langle K. E. \rangle$ is the average kinetic energy, x_i are the coordinates of the system and F_i is corresponding component of force, arising both from forces within the system and external forces. Averill²⁹ has shown

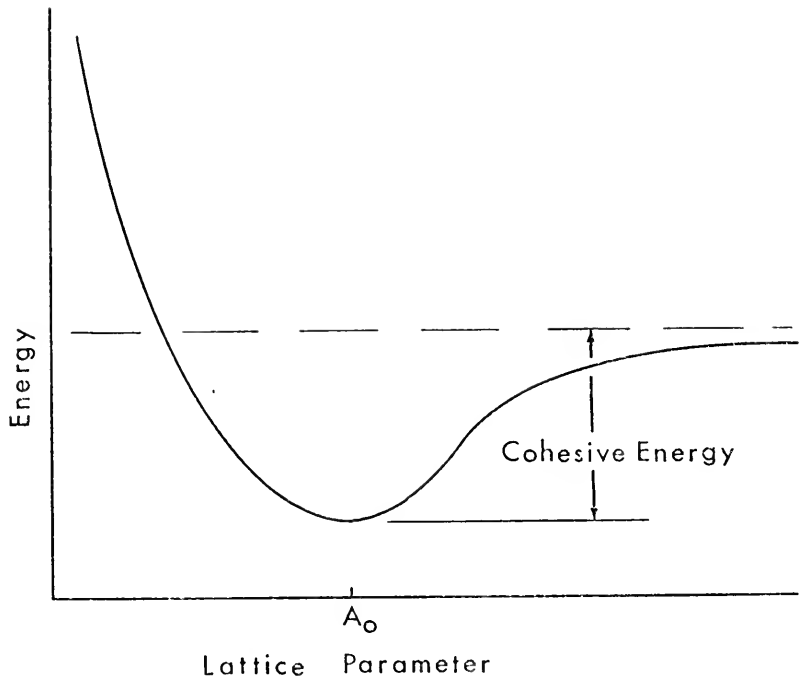


Figure 2.2. Qualitative graph of the ground state total energy of a crystal as a function of the lattice parameter.

that for the X_α method in the "muffin tin" approximation, the forces within the system result in a term given as

$$\left[\sum_i x_i F_{in_i} \right]_{av} = < P. E. > \quad (2.22)$$

where $<P. E. >$ is the average potential energy, and the external forces result in a term representing the volume times the pressure external to the system which is required to "hold" it in the assumed configuration,

The pressure, P , is given by

$$P = \frac{1}{3V} \left[<P. E. > + 2 <K. E. > \right] \quad (2.23)$$

where V is the volume and $P = 0$ corresponds to the virial coefficient equal to 1. This pressure is then determined as a function of α and that α selected that yields zero pressure at the experimental lattice parameter. This does not require quite so many calculations, but the calculations are much more difficult to carry to convergence; the requirement is now that the calculated pressure be stable upon proceeding from one iteration to the next. Obviously, one method is about as involved as the other. However, the latter method was used in the calculation presented here.

2.3 Potentials

The crystal potential used in these self-consistent APW calculations is of the "muffin tin" type, as mentioned in Sec. 1.2; that is, it is spherically symmetric within the non-overlapping spheres surrounding each atom and constant between spheres. The radii of these spheres, called APW spheres, are equal to one half the first

nearest neighbor distance. This insures that the spheres will contain the largest fraction of the Wigner-Seitz cell volume associated with each atom, without overlapping. In practice, it is found that the larger this fraction, the better the "muffin tin" potential approximates the exact one.

The coulomb part of the starting potential used in the self-consistent procedure is generated by a superposition of the coulomb part of the atomic potentials of the first few nearest neighbors, spherically averaged about the central atom. This is achieved by expanding the spherically symmetric atomic coulomb potentials of the neighboring atoms about the center atom by use of the alpha-function expansion suggested by Löwdin,³⁰ as described by Mattheiss.³¹ In metals, including contributions from the first four nearest neighbors, usually gives the required convergence of this expansion. The coulomb part of the constant potential between APW spheres is set equal to the average of the superposed coulomb potential in the region between the sphere and the Wigner-Seitz cell boundary.

The exchange portion of this starting potential is determined by the $X\alpha$ approximation, using a crystal charge density in which the contribution of neighboring atoms have been included by use of the same expansion used to expand the superposed coulomb potential. The exchange term in the constant potential is determined by

$$V_{ox} = -6\alpha \left[\frac{3}{8\pi} \rho_c \right]^{\frac{1}{3}} \quad (2.24)$$

where ρ_c is the constant part of a "muffin tin" charge density and is determined by requiring each Wigner-Seitz cell to be electrically neutral.

To determine the potential for the second and following iterations, the charge density resulting from the previous iteration is forced into a "muffin tin" form, as mentioned above. The coulomb part of the potential inside a sphere is evaluated using the spherically symmetric part of the charge density in an integral solution to the Poisson equation given as

$$V_c(r) = -\frac{2Z}{r} + \frac{2}{r} \int_0^r \rho(r') dr' - 2 \int_r^{R_s} \frac{\rho(r')}{r'} dr' + C \quad (2.25)$$

where R_s is the APW sphere radius and C is a constant of integration, needed only if the potential function is to be located with respect to the absolute zero of energy. The total potential function contains a finite discontinuity at R_s , the coulomb part of which is determined by use of the Ewald potential method as described by Slater and DeCicco.³² Solution of this problem insures that account is taken of the effects of all nuclei and "muffin tin" charge densities located exterior to the cell for which V_c is being computed.

The exchange term is determined, as in the superposed case, by the $X\alpha$ approximation. The discontinuity in this term at R_s is defined as the difference between the exchange corresponding to the spherically symmetric charge density within the spheres evaluated at R_s and the exchange corresponding to the uniform charge distribution

between spheres.

The total potential function is then given as the sum of the coulomb and exchange terms,

$$V'(r) = V_c(r) + V_x(r) \quad (2.26)$$

with a total discontinuity at R_s equal to the sum of the coulomb and exchange discontinuities. The potential V_{APW} used in the APW calculations, for convenience, is shifted by a constant V_0' so that the constant potential between spheres is zero, and is given by

$$V_{APW}(r) \equiv V'(r) = V_0' \quad (2.27)$$

where the primes are used to indicate that these potentials are not located with respect to the absolute zero of energy at infinity as is the case of the atomic potential function, and the case of the superposed potential used as a starting potential.

DeCicco¹¹ has suggested a method to correct this potential such that it will be in terms of the absolute values of energy. This method is based on the argument that the change in the potential at any point, in going from the initial to a final iteration, is completely determined by the change in the charge distributions. The change in the coulomb part of the potential at any point is given as

$$\delta V(\underline{r}) = 2 \int \frac{\delta \rho(\underline{r}')}{|\underline{r} - \underline{r}'|} d^3 r' \quad (2.28)$$

where the integration is to be performed over the entire solid. However, with the proper choice of cells over which the integral is evaluated, it

can be made to converge rapidly. A further simplification is achieved by evaluating the change in the coulomb potential at a point between spheres where only the Ewald charge distribution (assuming $\delta \rho$ is of "muffin tin" form) contributes to the constant potential and need be considered. This will yield the change in the constant part of the coulomb potential between the initial and final iteration, which is just the correction needed to locate the final potential with respect to the absolute zero of energy.

It can be shown that if the change in coulomb potential is evaluated at $\underline{r} = (111)A_0/4$ in the FCC structure, the Ewald method of solving the potential problem can be used to yield

$$\delta V_0 = V_{0e}' + \delta V'((111)A_0/4) - V_e'((111)A_0/4) \quad (2.29)$$

where V_{0e}' is the change in the average Ewald potential between spheres, $V_e'((111)A_0/4)$ is the change of the Ewald potential at $\underline{r} = (111)A_0/4$, and $\delta V((111)A_0/4)$ is the change in the coulomb potential at the point $(111)A_0/4$ in going from the initial to the final iteration. The values of V_{0e}' and $V_e'((111)A_0/4)$ for an FCC structure are determined by Slater and DeCicco³² to be given by

$$V_{0e}' = \frac{2 \delta Q}{A_0} \quad (0.8163) \quad (2.30)$$

and

$$V_e' = \left((111)A_0/4 \right) = \frac{2 \delta Q}{A_0} \quad (0.8019) \quad (2.31)$$

where A_0 is the lattice constant in Bohr radii and δQ is evaluated by subtracting the Ewald charge for the initial iteration from that of the

final iteration. DeCicco¹¹ has also evaluated $\delta V ((111)A_0/4)$ for an FCC structure and found it to be given by

$$\delta V \left((111)A_0/4 \right) = \frac{2 \delta Q}{A_0} (0.2796). \quad (2.32)$$

Substituting these values into Eq. (2.29) yields

$$\delta V_{0e} = \frac{2 \delta Q}{A_0} (0.8163 + 0.2796 - 0.8019)$$

or

$$\delta V_{0e} = \frac{2 \delta Q}{A_0} (0.2940). \quad (2.33)$$

The constant coulomb potential V_{0c} for the final iteration, located with respect to the absolute zero of energy, is then given by

$$V_{0c} = V_{0c} (\text{SFA}) + \delta V_{0e} \quad (2.34)$$

where $V_{0c} (\text{SFA})$ is the coulomb part of the constant potential for the superposed free atom case. The total constant potential is then given as

$$V_0 = V_{0c} + V_{0x} \quad (2.35)$$

where V_{0x} is the exchange part of the constant potential.

2.4 Total Energy and Cohesive Energy

If the $X\alpha$ approximation to the exchange potential is used, the expression for the total energy of a crystal, as described by Rudge,³³ may be written as

$$E = V_{nn} + \sum_i \int d^3 \underline{r}_1 U_i^*(\underline{r}_1) \left[-\nabla^2 + V_{ne}(\underline{r}_1) + \frac{1}{2} V_{ee}(\underline{r}_1) + \frac{1}{2} \left(\frac{3}{2} \alpha \right) V_{ex}(\underline{r}_1) \right] U_i(\underline{r}_1) \quad (2.36)$$

where

$$V_{nn} = \sum_{\substack{a, b \\ a \neq b}} \frac{Z_a Z_b}{|\underline{R}_a - \underline{R}_b|} = (\text{Nuclear-Nuclear Interaction})$$

$$-\nabla^2 = (\text{Electron Kinetic Energy})$$

$$V_{ne}(\underline{r}_1) = \sum_a \frac{2Z_a}{|\underline{R}_a - \underline{r}_1|} = (\text{Nuclear-Electron Coulomb Potential})$$

$$V_{ee}(\underline{r}_1) = \int d^3 \underline{r}_2 \frac{2\rho(\underline{r}_2)}{|\underline{r}_1 - \underline{r}_2|} = (\text{Electron-Electron Coulomb Potential})$$

$$V_{ex}(\underline{r}_1) = -6 \left[\frac{3}{8\pi} \rho(\underline{r}_1) \right]^{\frac{1}{3}} = (\text{Average Free Electron Exchange})$$

and

$$\rho(\underline{r}_1) = \sum_j U_j^*(\underline{r}_1) U_j(\underline{r}_1) = (\text{Total Electron Density})$$

The one-electron Schrödinger equation can be used to eliminate the

$-\nabla^2$ term and the expression rewritten as

$$\begin{aligned} E = & \left[\sum_i \epsilon_i \int d^3 \underline{r}_1 \left[V_{ne}(\underline{r}_1) + V_{ee}^0(\underline{r}_1) + \alpha V_{ex}^0(\underline{r}_1) \right] \rho(\underline{r}_1) \right] \\ & + \left[\frac{1}{2} \int d^3 \underline{r}_1 \left[V_{ne}(\underline{r}_1) + V_{ee}(\underline{r}_1) + \frac{3}{2} \alpha V_{ex}(\underline{r}_1) \right] \rho(\underline{r}_1) \right] \\ & + \left[\frac{1}{2} \int d^3 \underline{r}_1 V_{ne}(\underline{r}_1) \rho(\underline{r}_1) + V_{nn} \right] \end{aligned} \quad (2.37)$$

where the superscript 0 on V_{ee}^0 and V_{ex}^0 indicates that these potential

terms are evaluated for the charge density from the previous iteration,

whereas the other potentials terms are derived for the charge density resulting from the final iteration. With Eq. (2.37) grouped this way, the first term is the average kinetic energy of the electrons $(KE)_{av}$ and the last two represent the average potential energy $(PE)_{av}$. It has been shown by DeCicco¹¹ that the last term can be written as

$$\left[\frac{1}{2} \int d^3r_1 V_{ne}(r_1) \rho(r) + V_{nn} \right] = \frac{1}{2} \sum_a Z_a V_{a0} \quad (2.38)$$

where V_{a0} is the electrostatic potential at the ath nucleus due to all of the other charge in the crystal.

Because of the translational symmetry of the crystal structure, this expression can be written in terms of N , the number of total cells in the crystal, times the total energy per Wigner-Seitz cell. The expression for the total energy per cell, in the case of one atom per cell, can be written

$$E/N = \left[\sum_{cell} \epsilon'_i - \int_{cell} V'(r) \rho(r) dr \right] + \left[\frac{1}{2} \int_{cell} [V_{ne}(r) + V_{ee}(r) + \frac{3}{2} \alpha V_{ex}(r)] \rho(r) dr + \frac{Z}{2} V_0 \right] \quad (2.39)$$

where $\rho(r)$ is the radial electronic charge density and the primes on ϵ'_i and $V'(r)$ indicate that both are evaluated with respect to zero constant potential between spheres. The potentials in the second term can be written

$$V_{ne}(r) = - \frac{2Z}{r}$$

$$V_{ee}(r) = \frac{2}{r} \int_0^r \rho(r') dr' + 2 \int_r^{R_s} \frac{\rho(r')}{r'} dr' + C$$

$$V_{\text{ex}}(r) = -6 \left[\frac{3}{8\pi} \rho(r) \right]^{\frac{1}{3}}$$

and

$$V_0 = -2 \int_0^{R_s} \frac{\rho(r')}{r'} dr' + C \quad (2.40)$$

where C is the undetermined constant of integration that represents the effects of all the charge outside of the APW sphere. The V_0 term can be written

$$\frac{Z}{2} V_0 = -Z \int_0^{R_s} \frac{\rho(r')}{r'} dr' + \frac{Z}{2} C$$

while the term involving C in the preceding integral is given by

$$\frac{C}{2} \int_{\text{cell}} \rho(r) dr = -\frac{Z}{2} C. \quad (2.41)$$

Therefore, the terms depending on the constant value of the potentials cancel and the total energy is independent of the absolute zero of energy for the potential functions.

The cohesive energy (E_c) is defined as³⁴

$$E_c \equiv E_{\text{FA}} - E/N \quad (2.42)$$

where E_{FA} is the ground state total energy of the free atom. This is shown graphically in Fig. 2.2 of Sec. 2.2 above.

2.5 Pressure and Compressibility

There are two ways to determine the pressure in a crystal.

The first method involves the use of the virial theorem associated with the calculation for a metal, in which both the $X\alpha$ and "muffin tin"

approximations are used, as described in Sec. 2.2. With this method the pressure is given in Eq. (2.23) as

$$P = \frac{1}{3V} \left[2 (KE)_{av} + (PE)_{av} \right].$$

If the $(KE)_{av}$ and $(PE)_{av}$ are expressed in Rydbergs (Ry), and V is expressed in cubic atomic units (cau), the pressure in kilobars (Kb) is given by

$$P = (4.8959 \times 10^4) \frac{1}{V} \left[2 (KE)_{av} + (PE)_{av} \right]. \quad (2.43)$$

The second method of determining the pressure is to generate the curve for energy vs. volume, by evaluating the energy for several values of the lattice constant. The pressure is then

$$P = - \frac{dE}{dV} \quad (2.44)$$

which can be evaluated for any point on the curve by numerical methods.

As in the first method, the pressure in kilobars (kb) is given by

$$P = (-1.4688 \times 10^5) \frac{dE}{dV} \quad (2.45)$$

with the energy and volume expressed in atomic units.

The compressibility (K) given as

$$K = - \frac{1}{V} \frac{dV}{dP} \quad (2.46)$$

is equal to the reciprocal of the bulk modulus, given by

$$B = \frac{1}{K} = - V \frac{dP}{dV}. \quad (2.47)$$

Substituting for P in this equation from Eq. (2.44), yields

$$B = V \frac{d^2 E}{dV^2}. \quad (2.48)$$

Therefore, the compressibility can be evaluated at any value of the lattice constant by numerically evaluating the second derivative of the energy vs. volume curve generated for use in the second method of determining pressure, described above.

CHAPTER III

RESULTS OF THE CALCULATION FOR COPPER

3.1 Determining α of the $X\alpha$ Method

The α used in this calculation was determined to be the one that would yield a virial coefficient equal to unity, as described in Sec. 2.2. This was done by evaluating the pressure for a series of self-consistent APW calculations, each for a different value of α . The pressure as a function of α from these calculations was then plotted, and the α determined that would yield zero pressure at the experimentally observed lattice constant (A_0). The pressure for each calculation was determined by

$$P = \frac{1}{3V} \left[2 (\text{K. E.})_{\text{av}} + (\text{P. E.})_{\text{av}} \right] \quad (3.1)$$

which comes from the virial theorem as described in Sec. 2.5.

Each self-consistent calculation was done using a 500 point linear radial mesh (for integration of the radial Schrödinger equation) and for 2048 points in the first Brillouin zone. The self-consistency criterion used in these calculations was that the resulting pressure vary by less than 1 Kb between two successive iterations. This required from 8 to 10 iterations in most cases, with each iteration taking about 5 minutes of computer time on the CDC 7600. It is of interest to note that the variation in total energy between two successive iterations was about 10^{-6} Ry when the pressure criterion was satisfied.

The resulting pressures for four such calculations are given in Table 3.1, along with the kinetic, potential, and total energies. Pressure as a function of α is plotted in Fig. 3.1, while total energy as a function of α , for the same four calculations, is given in Fig. 3.2. The total energy is very nearly a linear function of α , as is the case in atomic $X\alpha$ calculations, while the pressure is not. However, a smooth curve can be drawn through the average of these data points on the pressure vs. α plot in Fig. 3.1; this predicts an α of about 0.7225 for zero pressure. This was the value of α used to evaluate the total energy as a function of lattice parameter and the resulting pressures and compressibility.

3.2 Total Energy and Cohesive Energy Results

Calculations were made for six values of the lattice parameter (A) of FCC copper, each with $\alpha = 0.7225$. These were the lattice parameter corresponding to the experimentally determined Wigner-Seitz cell volume (V_0) and lattice parameters corresponding to 10% and 20% reductions of this volume and 10%, 20%, and 60% expansions of this volume. Each calculation, with the exception of the 60% expansion, was converged until the pressure, as determined using the virial theorem (Eq. 2.43), varied by less than 1 Kb between two successive iterations. This usually took from 10 to 15 iterations, at five minutes an iteration on a CDC 7600 computer. As in the calculations discussed

TABLE 3.1.

The pressure, potential energy, kinetic energy, and total energy for four self-consistent APW calculations on copper, with different values of α .

α	Pressure (Kb)	Potential Energy (Ry)	Kinetic Energy (Ry)	Total Energy (Ry)
0.70000	33.70	-6553.880469	3276.967354	-3276.913115
0.70635	24.35	-6556.226508	3278.132847	-3278.093661
0.72000	3.64	-6561.271765	3280.638812	-3280.632953
0.77000	-60.34	-6579.806760	3289.854829	-3289.951931

Figure 3.1. Pressure vs. α of the $X\alpha$ method, for copper.

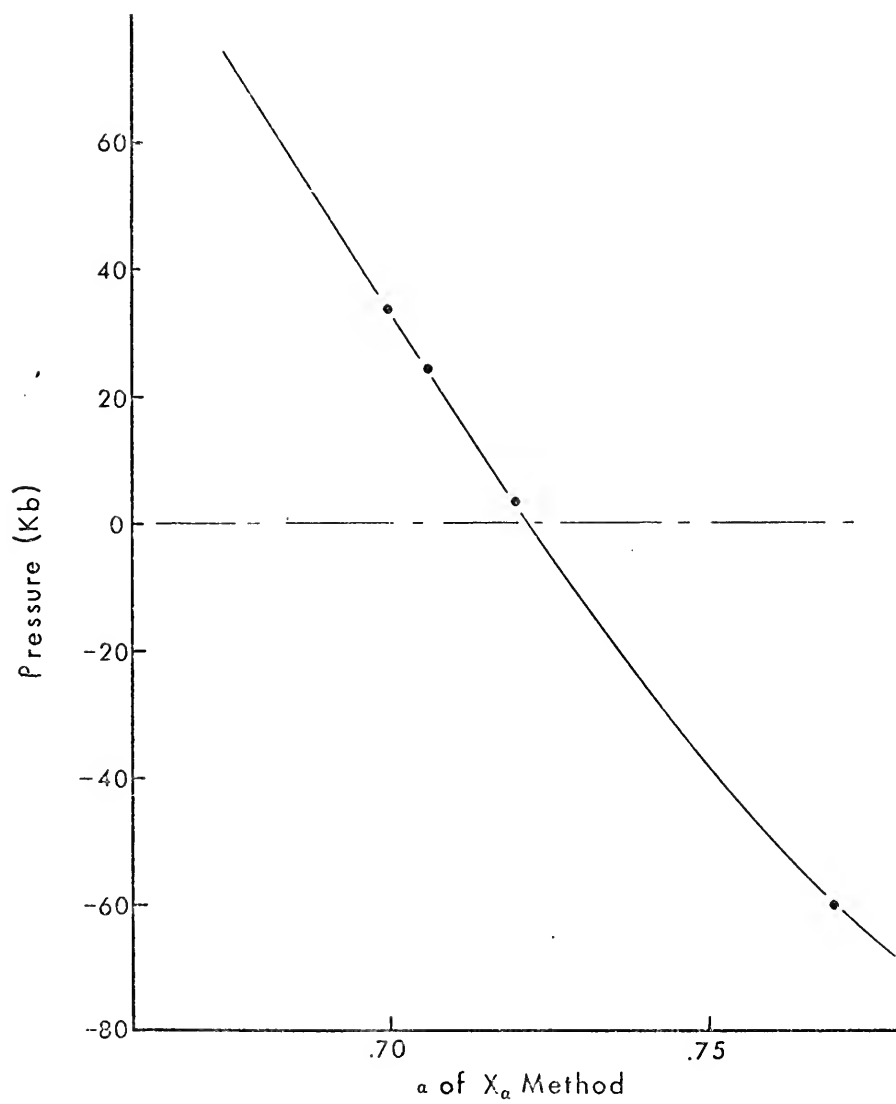


Figure 3.1

Figure 3.2. The total energy vs. α of the $X\alpha$ method for copper

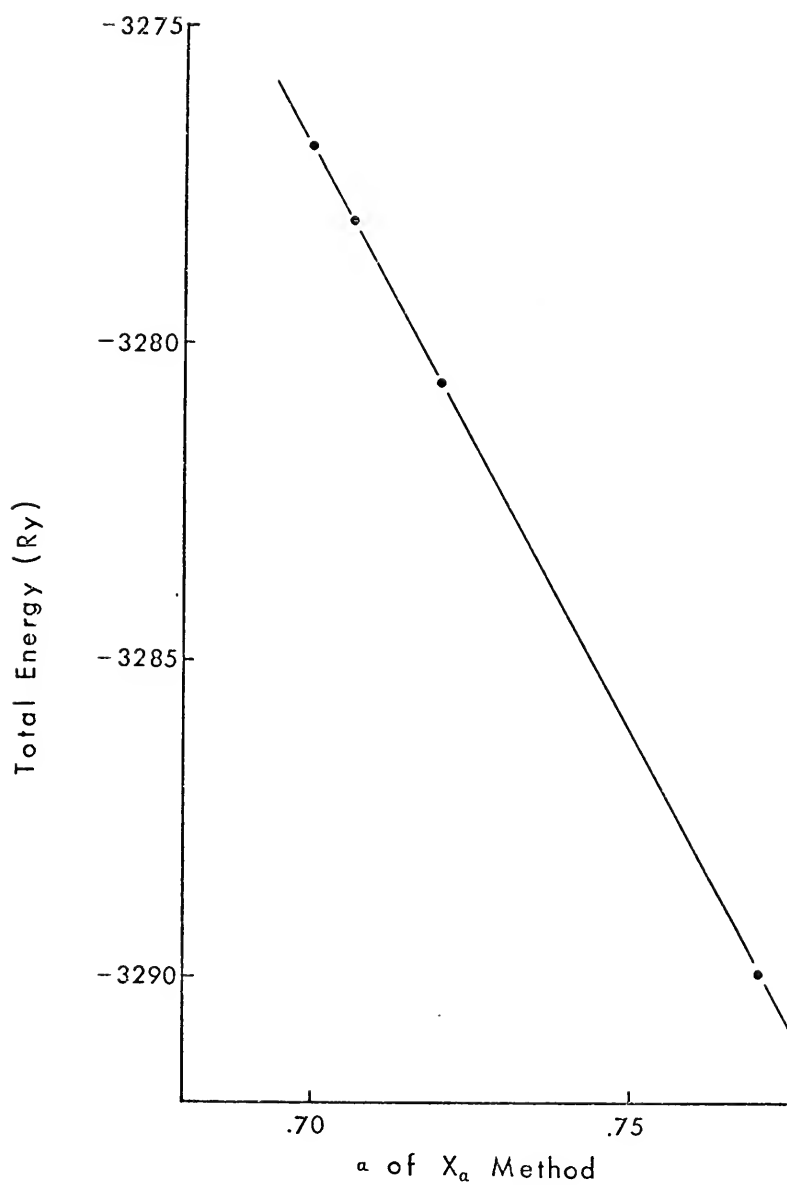


Figure 3.2

in the preceding section, when this convergence criterion was met, the change in total energy was about 10^{-6} Ry between two successive iterations. The calculation corresponding to 60% volume expansion was converged so that the total energy varied by less than 10^{-4} Ry between two successive iterations. Each calculation was done for 2048 points in the first Brillouin zone and used a 500 point linear radial mesh.

The total energies resulting from these calculations are given in Table 3.2. Also given are the volumes in cubic atomic units (cau) and the lattice parameters in atomic units (au). These data are plotted in Fig. 3.3, showing the total energy as a function of lattice parameter. This curve shows a definite minimum near the experimentally determined lattice parameter (A_0), as predicted by the results given in the preceding section (Sec. 3.1).

The cohesive energy was determined as the difference in the total energy at the minimum of the energy vs. lattice parameter curve in Fig. 3.3 and the statistical total energy for the atomic calculation using the same value of α , as described in Sec. 2.4. The atomic calculation for the 2S ground state was a non-spin-polarized Herman-Skillman¹² calculation using the $X\alpha$ exchange approximation. These total energies are approximately -3281.098 Ry and -3280.813 Ry for the metallic and atomic calculations, respectively. This gives a cohesive energy of 0.286 Ry, compared to the experimental value³⁴ of

TABLE 3.2

Total energy for six values of the lattice parameter for copper ($\alpha=0.7225$).

V/V_0	Volume (V) (au^3)	Lattice Parameter (A) (au)	Total Energy (Ry)
0.80	63.1256584	6.3205563	-3281.074352
0.90	71.0163639	6.5736434	-3281.093786
1.00	78.9070739	6.8086129	-3281.098246
1.10	86.7977809	7.0283957	-3281.094903
1.20	94.6884870	7.2352308	-3281.087333
1.60	126.2513250	7.9634021	-3281.044053
∞ (Free Atom)	∞	∞	-3280.812553

Figure 3.3. The total energy as a function of lattice parameter for copper ($\alpha = 0.7225$).

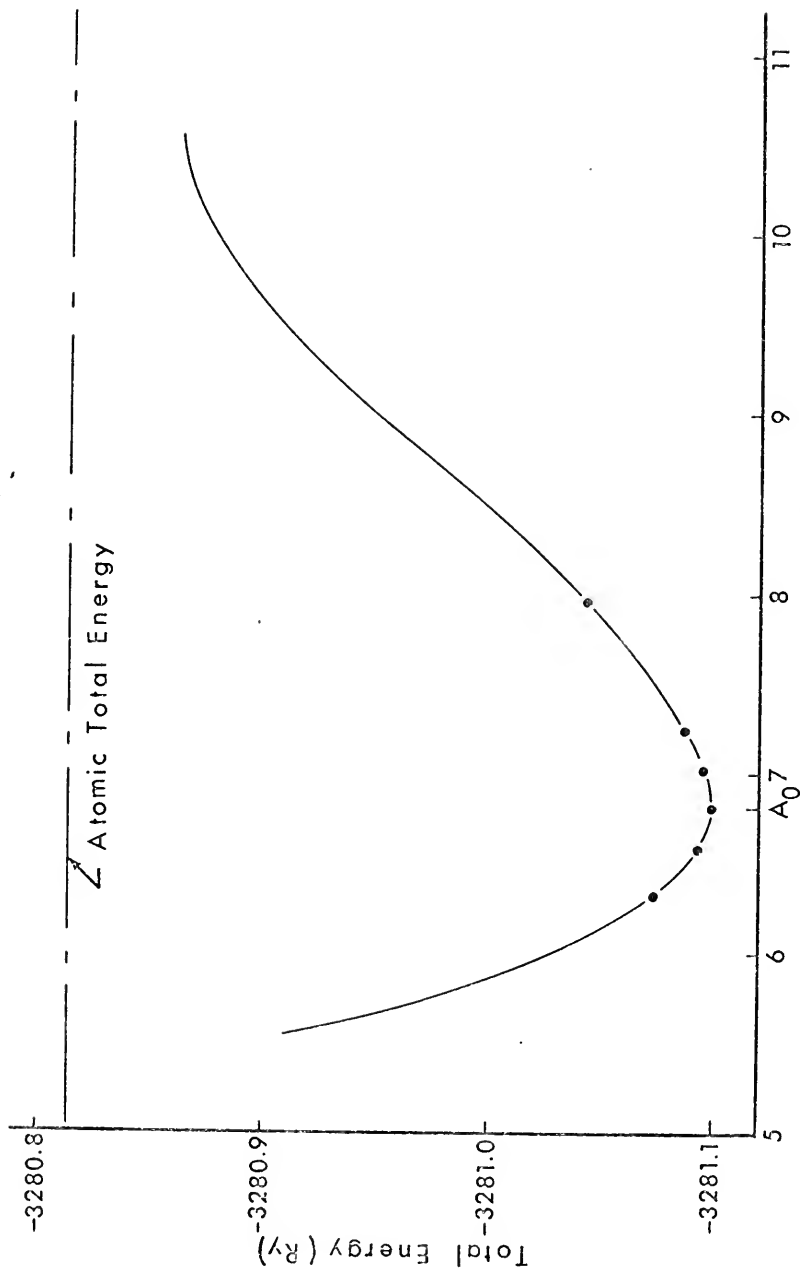


Figure 3.3

0.257 Ry. The fractional difference between this calculated value and the experimental value of cohesive energy is 0.112 or about 11%. This is fairly good agreement if one considers that the calculated value of cohesive energy is about 0.00001 of the total energies used to determine it.

3.3 Pressure and Compressibility

The total energy as a function of volume is shown in Fig. 3.4 for the first five calculations given in Table 3.2 of the preceding section. This covers only a small part of the entire curve near the minimum showing how the slope and curvature vary in that region.

The pressures at each of these five values of the volume for these calculations were determined using two different methods and are given in Table 3.3. The pressures given in the third column of this table were determined using Eq. (2.43) derived from the virial theorem as described in Sec. 2.5. The pressures given in the fourth column were determined as the negative of the first derivative of the total energy as a function of volume as given in Eq. (2.44) (evaluated for each value of the volume, also described in Sec. 2.5). Both sets of pressures are shown in Fig. 3.5, plotted as a function of volume. The agreement between the pressures determined by these two methods is obviously quite good.

The bulk modulus was evaluated using both curves shown in Fig. 3.5, and is determined as the volume times the negative of the

Figure 3.4. The total energy as a function of volume for copper, near the minimum ($\alpha = 0.7225$). (V is the volume and V_0 is the volume corresponding to the experiment lattice parameter.)

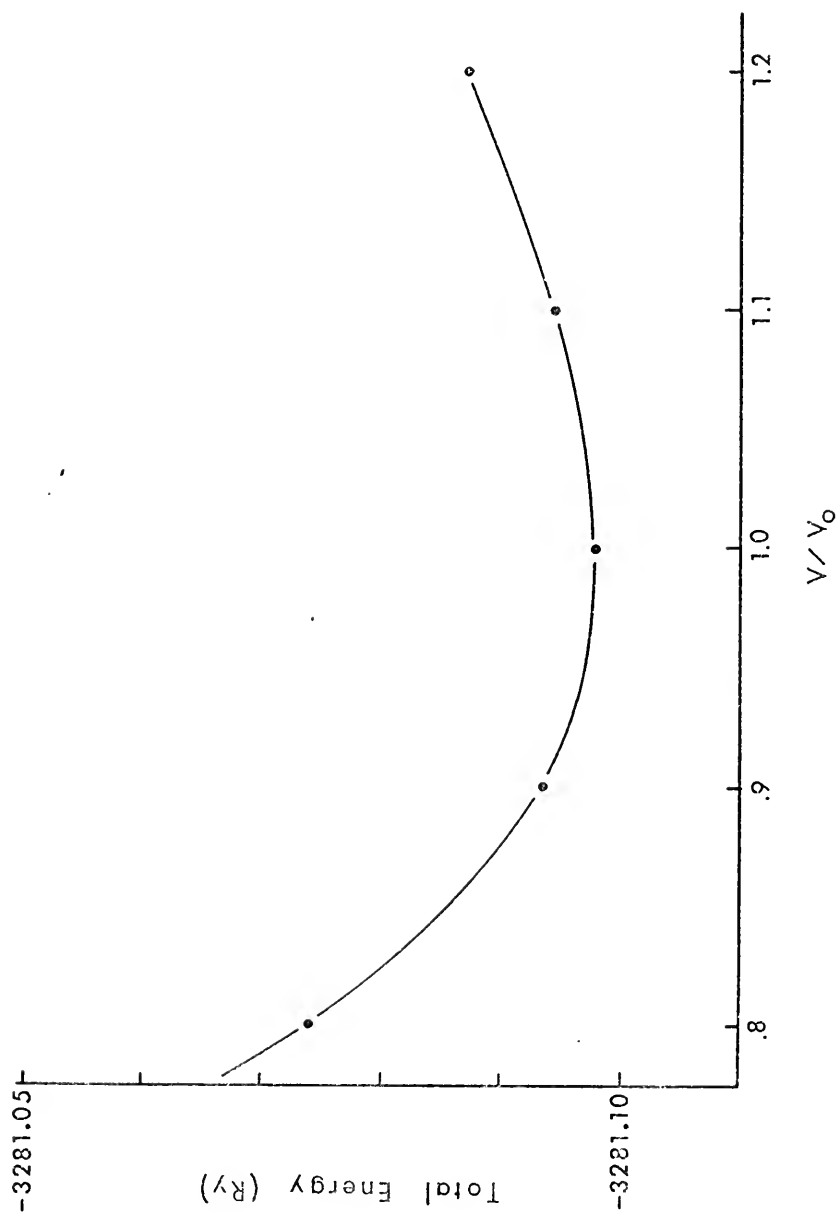


Figure 3.4

TABLE 3.3

The pressure for five values of the cell volume of FCC copper, evaluated using the virial theorem (vt) and the slope of the energy vs. volume curve at V_0 (E vs. V). (V_0 is the volume corresponding to the experimental lattice parameter.)

V/V_0	Volume (V) (cau)	Pressure (vt) (Kb)	Pressure (E vs. V) (Kb)
0.80	63.1256584	559.9	562.3
0.90	71.0163639	200.9	194.6
1.00	78.9070739	1.3	6.3
1.10	86.7977809	-105.9	-107.1
1.20	94.6884870	-169.3	-174.8

Figure 3.5. Pressure as a function of volume. The solid curve is for pressures determined using the virial theorem and the dashed curve is for pressures determined using the derivative of the energy vs volume curve at V_0 . (V_0 is the volume corresponding to the experimental lattice parameter.)

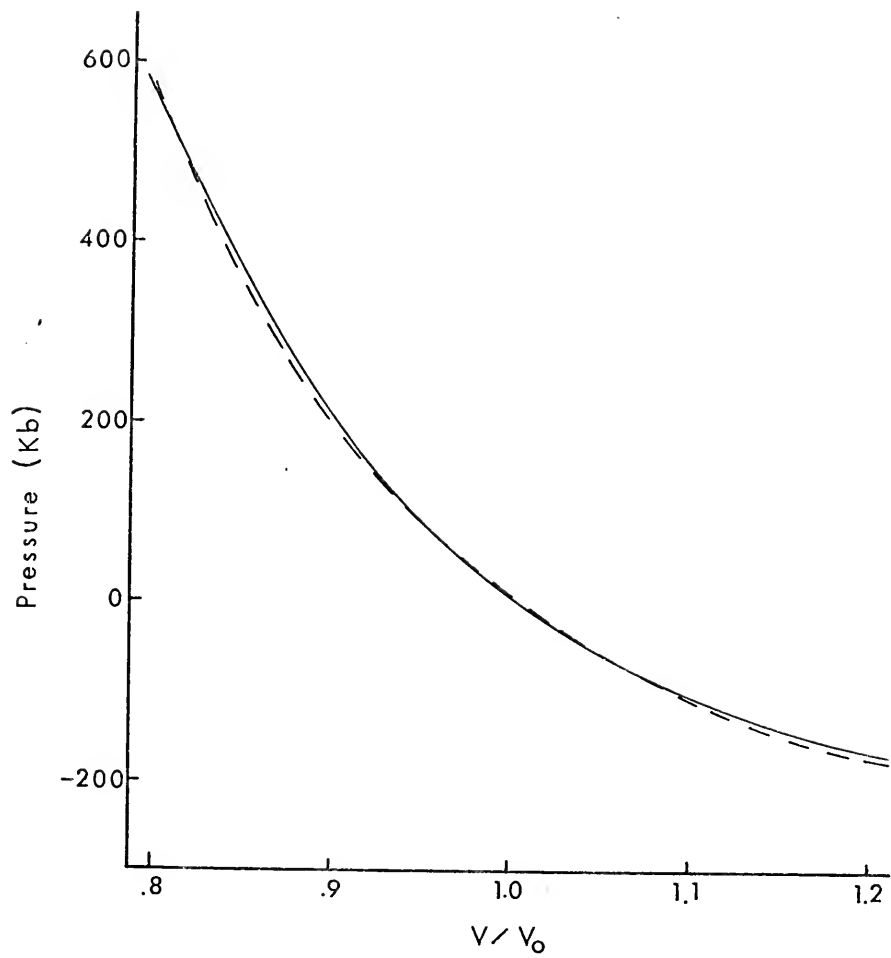


Figure 3.5

first derivative of the pressure as a function of volume evaluated at V_0 , using Eq. (2.47) as described in Sec. 2.5. The bulk modulus was also determined as the volume times the second derivative of the total energy as a function of volume evaluated at V_0 , as given in Eq. (2.48). This value of the bulk modulus was the same as that determined from the slope of the pressure vs. volume curve resulting from the first derivative of the energy as a function of volume. The only differences in these two values of the bulk modulus were attributed to the inaccuracies in the numerical methods used to evaluate the first and second derivatives, as would be expected.

The compressibility, which is the reciprocal of the bulk modulus, was determined to be $6.96 \times 10^{-4} \text{ Kb}^{-1}$ for the values of pressure obtained using the virial theorem, and $7.16 \times 10^{-4} \text{ Kb}^{-1}$ for the values of pressure obtained using the total energy as a function of volume. These two values differ from the experimental value³⁵ of $7.49 \times 10^{-4} \text{ Kb}^{-1}$, by 7% in the first case and 4% in the latter one, which is reasonably good agreement.

3.4 Energy Bands and Density of States

The energy bands for five calculations of copper for the lattice parameters corresponding to the experimental value and 10% and 20% volume expansion and compression are given in Figures 3.6, 3.7, 3.8, 3.9, and 3.10. The energy bands in these figures are shown

Figure 3.6 (a & b) Energy bands for FCC copper with $\alpha = 0.7225$ and $A = 6.321$ a.u. (c) Density of states for this calculation.

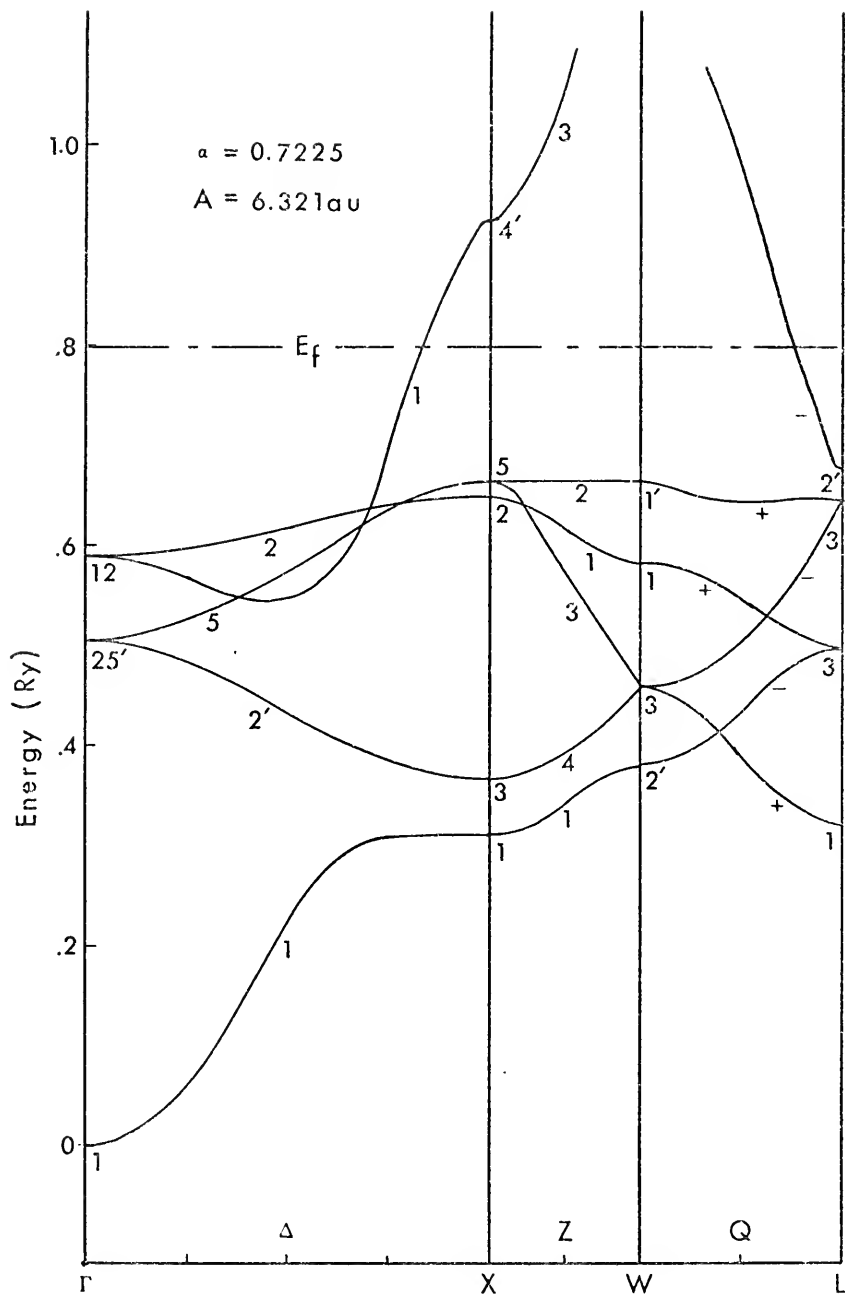


Figure 3.6a

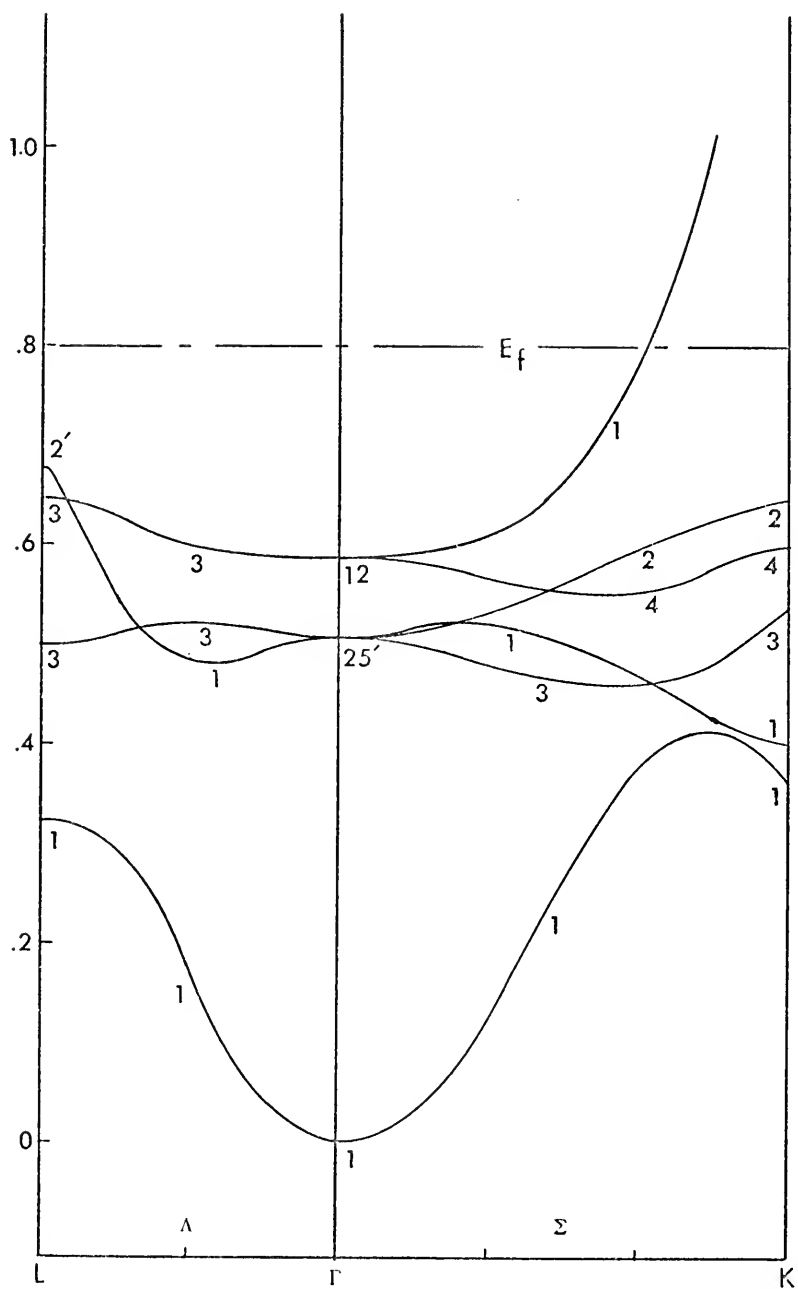


Figure 3.6b



Energy (Ry)
Figure 3.6c

Figure 3.7. (a & b) Energy bands for FCC copper with $\alpha = 0.7225$ and $A = 6.574$ a.u. (c) Density of states for this calculation.

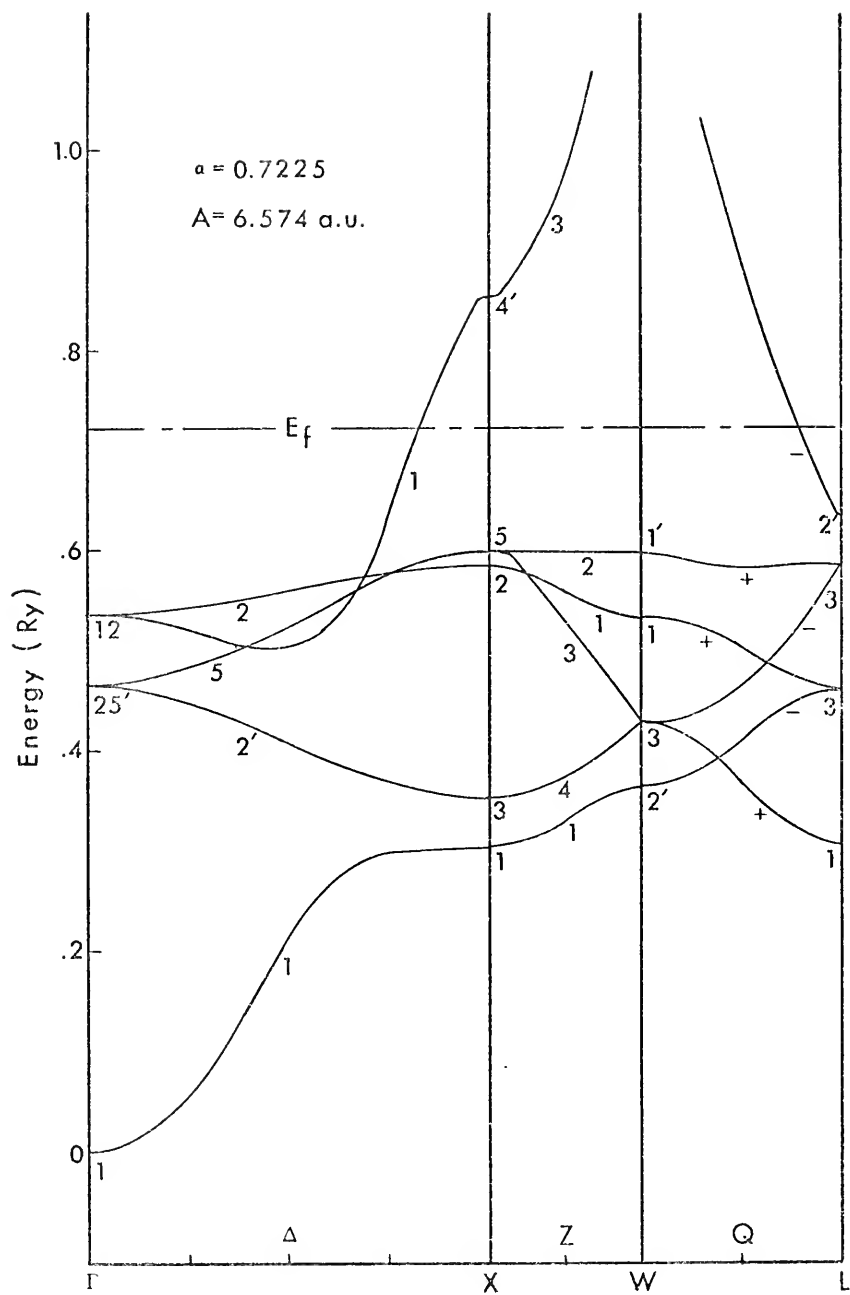


Figure 3.7a

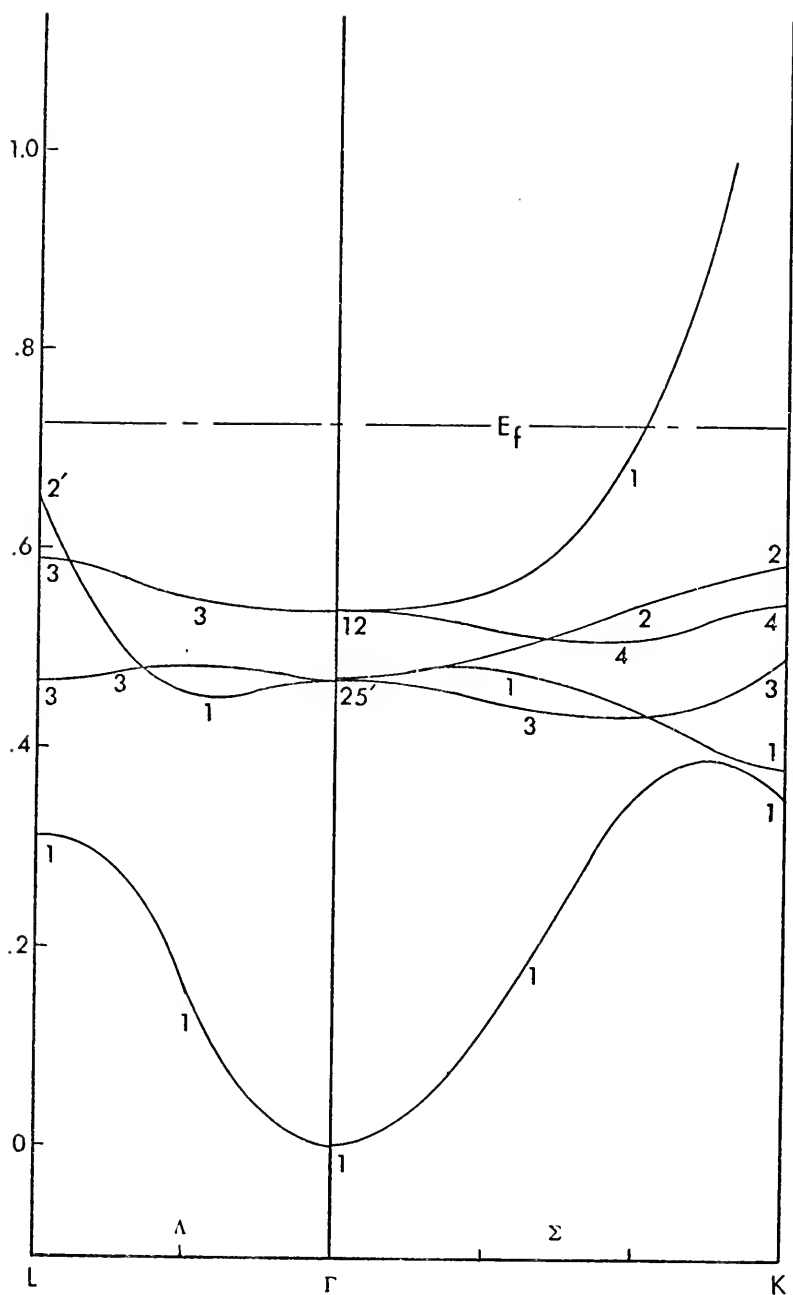


Figure 3.7b

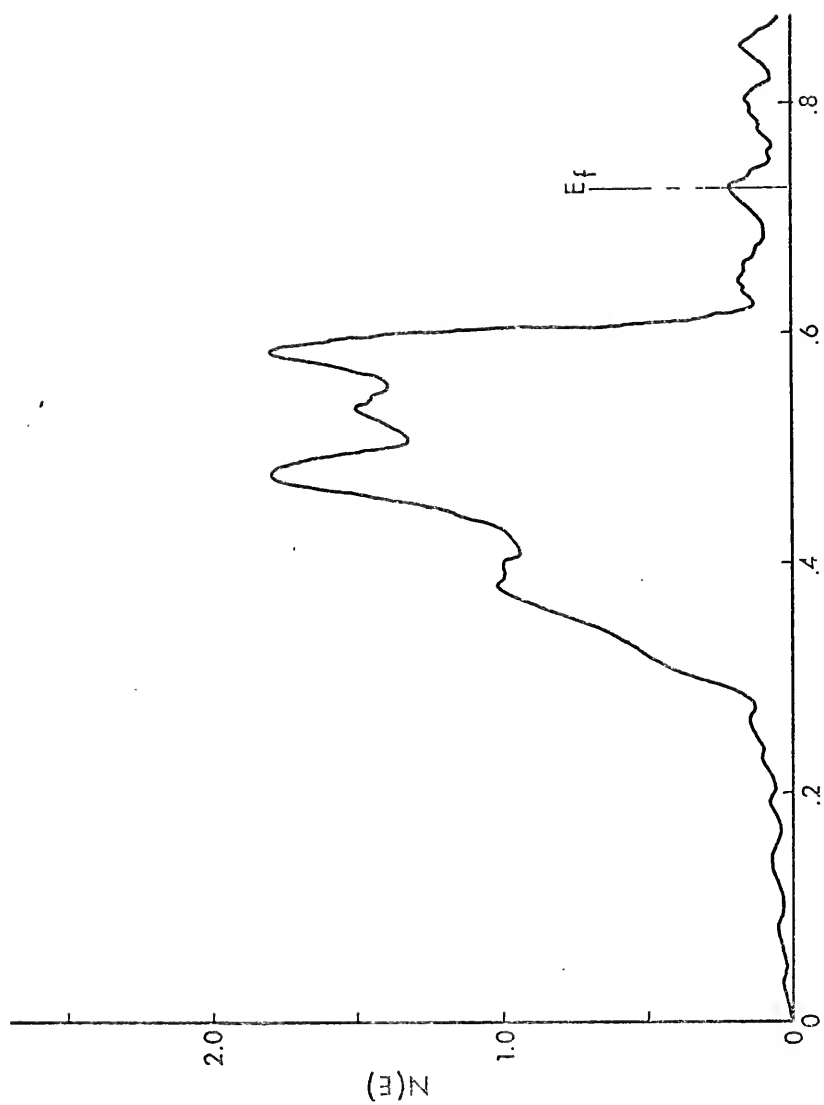


Figure 3.7c

Figure 3.8. (a & b) Energy bands for FCC copper with $\alpha = 0.7225$ and $A = 6.809$ a.u. (c) Density of states for this calculation.

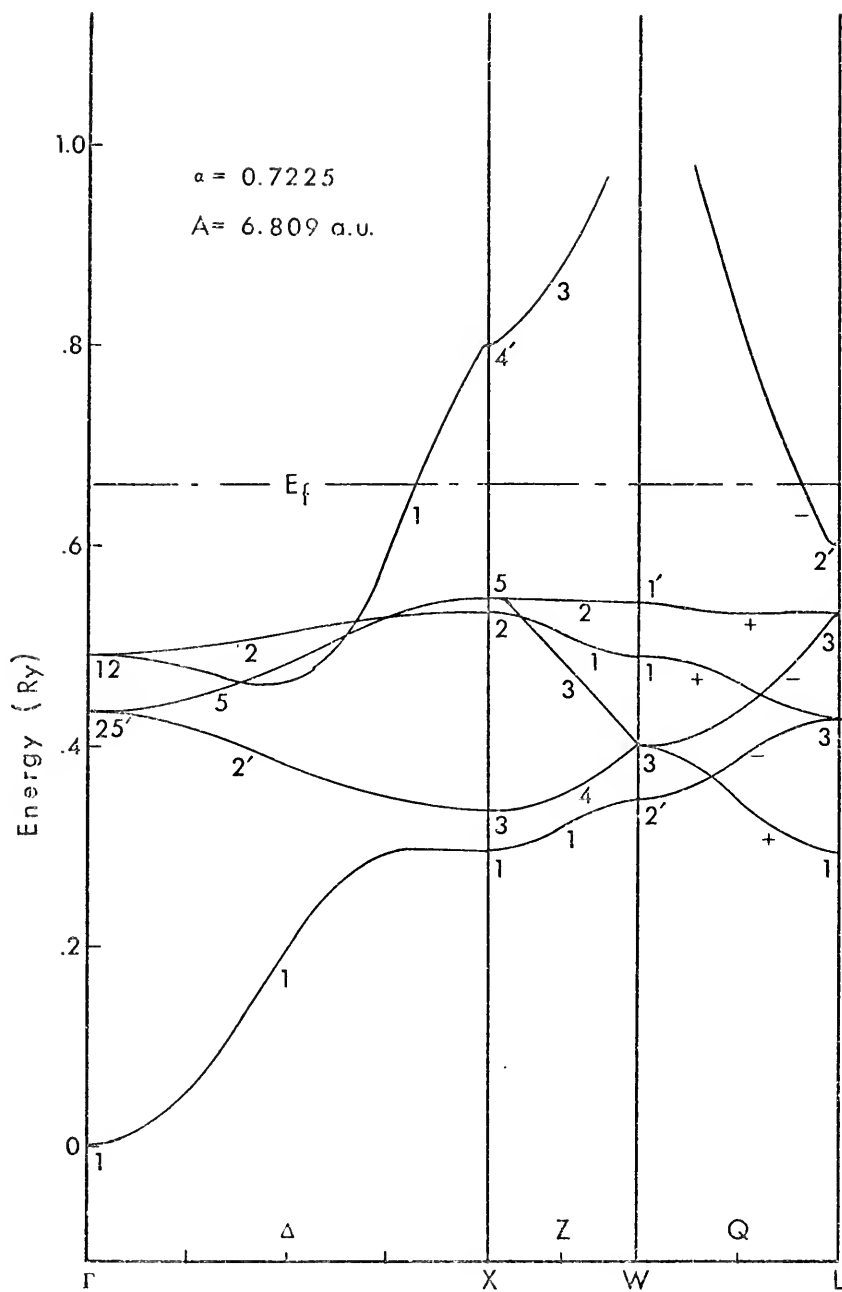


Figure 3.8a

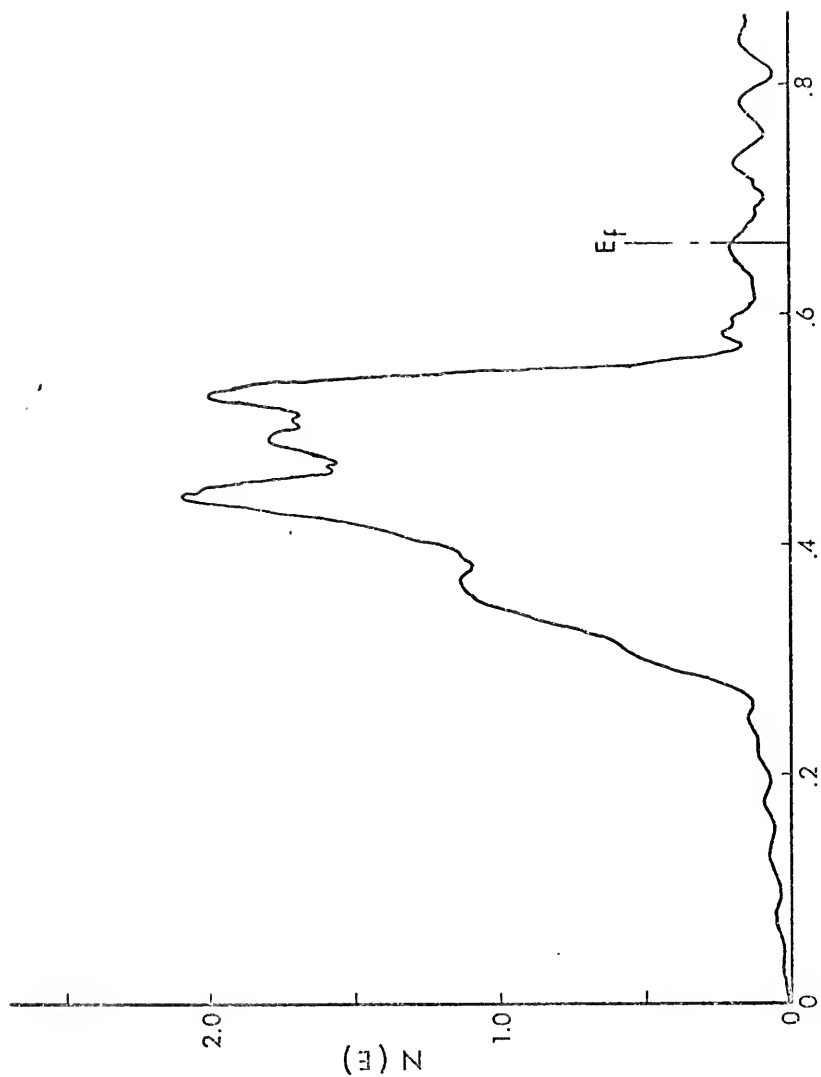


Figure 3.8c

Figure 3.9. (a & b) Energy bands for FCC copper with $\alpha = 0.7225$ and $A = 7.023$ a.u. (c) Density of states for this calculation.

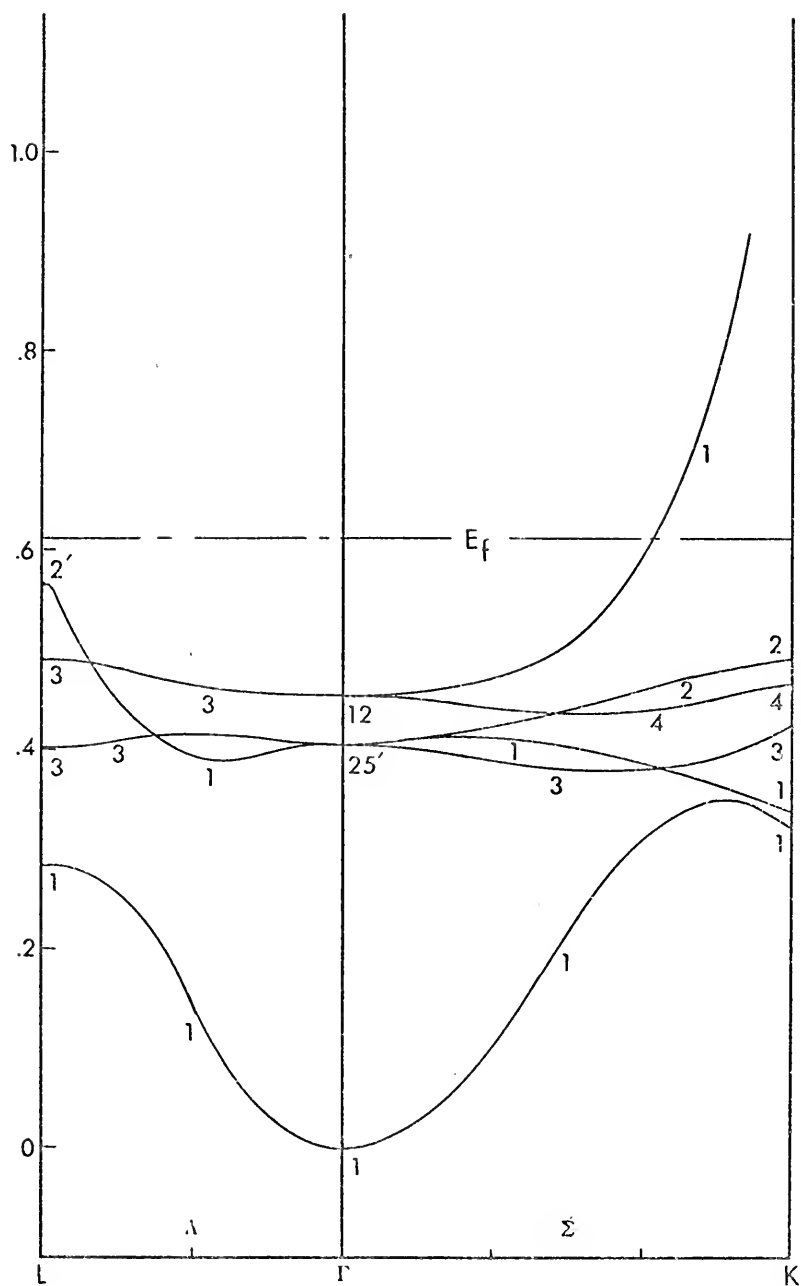


Figure 3.9b

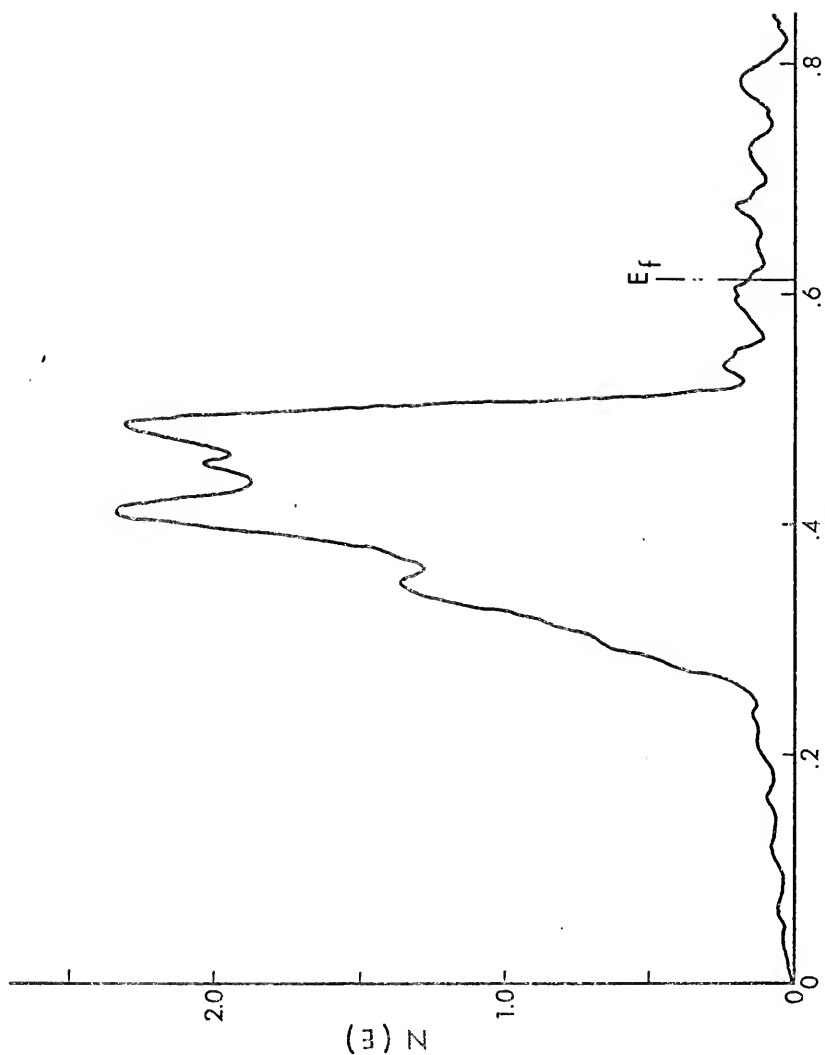


Figure 3.9c

Figure 3.10. (a & b) Energy bands for FCC copper with $\alpha = 0.7225$ and $A = 7.235$ a.u. (c) Density of states for this calculation.

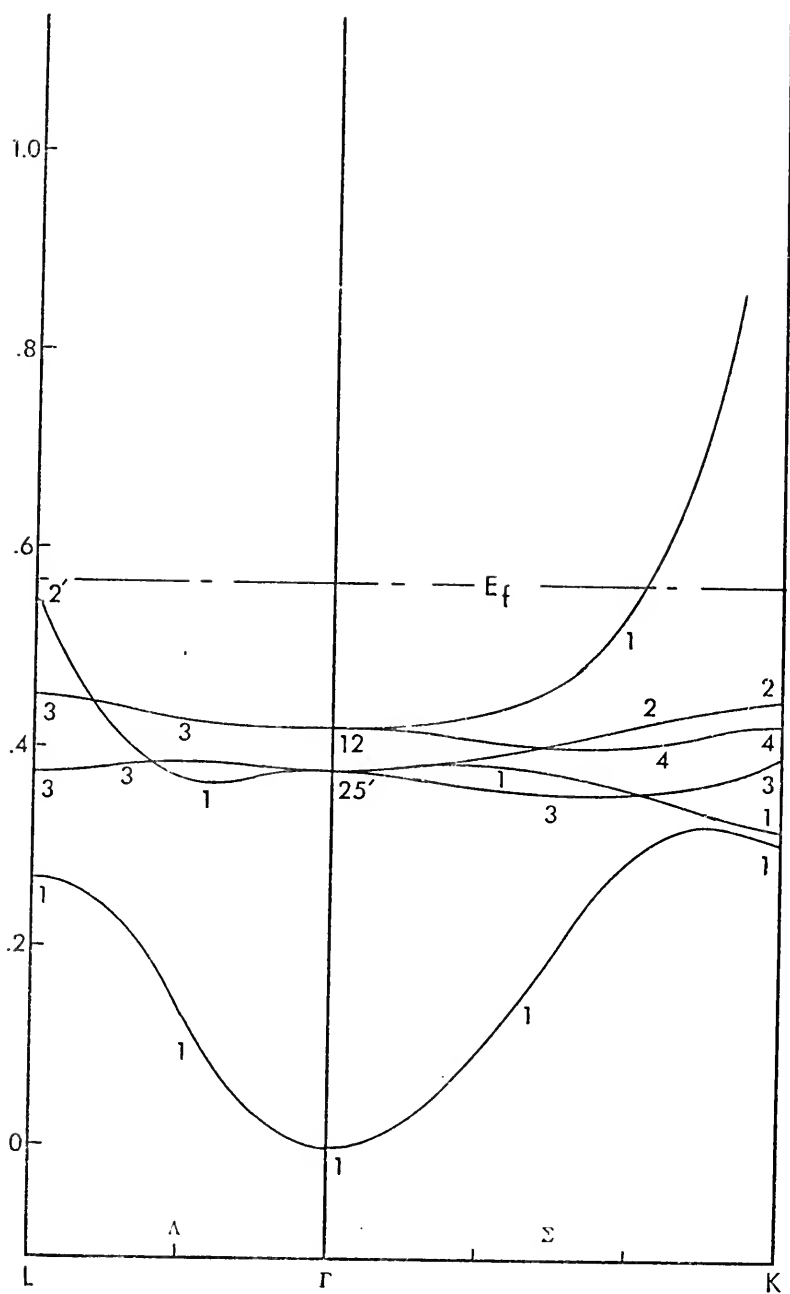


Figure 3.10b

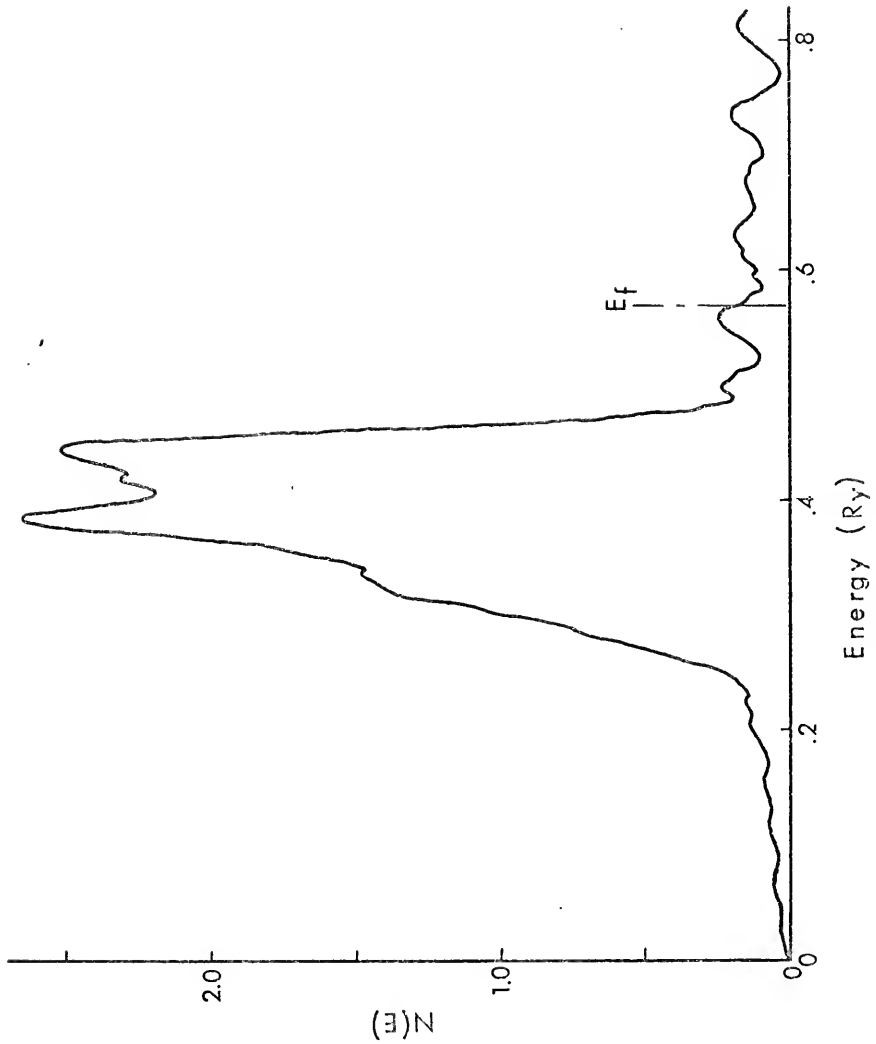


Figure 3.10c

in the directions of highest symmetry in the first Brillouin zone of the FCC structure. The value of α used for all five calculations was 0.7225. The corresponding density of states for each calculation is also given.

Energy differences for these calculations, that represent the bandwidths and relative locations of the bands with respect to each other and with respect to the Fermi energy, are given in Table 3.4. The energy differences given as $(\Gamma_{25'} - \Gamma_1)$ and $(X_5 - \Gamma_1)$ give the relative location of the d-band with respect to the bottom of the sp-band, while the differences $(E_f - X_5)$ and $(E_f - L_3)$ locate the top of the d-band with respect to the Fermi energy. The energy differences $(X_5 - X_1)$ and $(X_4' - \Gamma_1)$ give the bandwidths of the d-band and sp-band, respectively. $(E_f - L_2')$ represents the location of the high symmetry point with an eigenvalue nearest the Fermi energy. This energy difference also gives a measure of the "neck" radius of the copper Fermi surface.

A similar set of energy differences for experimental results, results of previous calculations, and results of present calculations for different values of α (at the equilibrium lattice constant) are given in Table C.1 in Appendix C, and are not included in this table.

The relative movements and changes in bandwidth of the bands as the lattice parameter is increased are as expected; namely, both the d-band and the sp-band narrow and the d-band moves toward the bottom of the sp-band. If one were to continue increasing the lattice

TABLE 3.4

Energy differences for states that indicate positions and widths of the sp-band and d-band (Ry). * ($\alpha = 0.7225$)

V/V_0	$\Gamma_{25}^{-1}-\Gamma_1$	$X_5^{-1}-\Gamma_1$	X_5-X_1	$X_4^{-1}-\Gamma_1$	E_f-X_5	E_f-L_3	E_f-L_2'
0.8	0.507	0.668	0.356	0.926	0.132	0.152	0.120
0.9	0.469	0.603	0.297	0.857	0.121	0.138	0.088
1.0	0.435	0.549	0.252	0.801	0.114	0.127	0.063
1.1	0.405	0.504	0.217	0.754	0.108	0.119	0.041
1.2	0.379	0.465	0.189	0.715	0.103	0.113	0.024

*Experimental results, results from previous calculations, and results from present calculations for various values of α are given in Table C.1 in Appendix C.

parameter, the d-band would continue to become narrower and eventually drop completely below the sp-band, approaching the 3d atomic state in the limit of infinite lattice parameter. The Fermi energy "follows" the d-band, moving toward the bottom of the sp-band faster than does the energy of the L_2' point, resulting in a decrease in the energy difference $(E_f - L_2')$ and a decrease in the "neck" radius of the copper Fermi surface.

In comparing the results given in Table 3.4 with experimental results, only those for the experimental lattice parameter ($V/V_0 = 1.0$) can be considered. For these results, the d-band appears to be too broad and too close to the Fermi energy when compared with the results of photoemission studies.³⁶⁻³⁸ The $(E_f - L_2')$ energy difference also appears too large when compared to the results of Spicer³⁶ or Lindau and Wallden.³⁹ However, the value of such comparisons is questionable. Nevertheless, the value of $(E_f - L_2')$ given here as 0.063 Ry is only slightly larger than the value of 0.061 Ry given by Janak et al.⁴⁰ as being the value that gives a "neck" radius in agreement with experiment.

CHAPTER IV

CONCLUSIONS

The main purpose of this dissertation was the evaluation of the $X\alpha$ exchange approximation as used in self-consistent APW calculations for a metal, such as metallic copper. To achieve this, the total energy as a function of lattice parameter was determined and these results were used to determine cohesive energy and compressibility. Comparison of these quantities with experimental results gives a measure of the accuracy of these calculations and some indication of the worth of the methods employed. Of course, a complete evaluation of the methods would involve a large number of calculations on a variety of materials; such other calculations have already been done by Averill^{26, 27} and Hattox.²⁸

To evaluate the results of the present work, we first consider the method proposed to determine the α that was used in the $X\alpha$ exchange approximation. As was pointed out in Sec. 3.1, the value of α that would give zero pressure at the experimentally determined lattice spacing was found to be 0.7225. The results given in Table 3.3 show that the calculated pressure at the experimental lattice spacing resulting from the use of this value of α was 1.3 Kb instead of zero as required. However, this represents a difference in the potential

energy and twice the kinetic energy of approximately 0.002 Ry. This is a very small fraction (on the order of 3×10^{-7}) of the 6562 Ry, which is the approximate magnitude of these two numbers. The virial coefficient, defined in Eq. (2.20) as the ratio of the negative of the potential to twice the kinetic energy, was 0.9999997 for this calculation, or very nearly 1.0, the desired value.

The total energy as a function of lattice parameter, as one would expect for this calculation, has a minimum very close to the experimentally determined lattice parameter, as can be seen in Figs. 3.3 and 3.4. The pressure of 6.3 Kb, given in Table 3.3, indicates that the minimum occurs slightly outside the experimental value. This is evident if one considers that 6.3 Kb represents a slope in the energy vs. volume curve of about -4×10^{-5} in atomic units.

The cohesive energy obtained from the calculation at the experimental lattice spacing with $\alpha = 0.7225$ was 0.286 Ry. This value is within 11% of the experimental value of 0.257 Ry, and is probably within the experimental accuracy of determining the cohesive energy at 0°K.

The energy bands for this calculation agree reasonably well with the results of photoemission studies given in Table C.1, though such direct comparisons are somewhat questionable. However, the resulting ($E_f - L_2$) energy difference of 0.063 Ry agrees very well with the 0.061 Ry given by Janak et al.⁴⁰ as being the value that corresponds

to a "neck" radius of the copper Fermi surface in agreement with experiment.

Probably the most significant results achieved in the present calculations were the agreement between the two sets of calculated values of the pressure as a function of lattice parameter and the values of the compressibility determined from these two sets of data. The agreement between these two sets of calculated pressures, given in Table 3.3, is evident in Fig. 3.5. The compressibilities determined from the slope of these two curves agree with the experimental value (to within 7% and 4%).

Hence, one can conclude that the $X\alpha$ method, as applied in these calculations, can be used to obtain total energy as a function of lattice parameter, cohesive energy, and compressibility that are in good agreement with experimental values. However, these results would have agreed with experiment just about as well, if the α that satisfied the virial theorem for the atomic calculation ($\alpha = 0.70635$) had been used in the present calculations, even though the minimum of the energy vs. lattice parameter curve would be slightly outside the experimentally determined lattice parameter, by approximately 0.5%. This indicates that, from a practical point of view, this value of α is probably the best one to use in a calculation of this type, as was the case for the calculations by Averill^{26, 27} and Hattox.²⁸

APPENDICES

APPENDIX A

METHODS OF IMPROVING THE ACCURACY OF THE LOGARITHMIC DERIVATIVES USED IN AN APW CALCULATION

A.1 Introduction

In using the APW method for calculating the energy-bands of a crystal, the determination of pressure and cohesive energy requires greater precision than is needed for determining just the energy bands $E(k)$. There are several obvious ways of improving accuracy, such as increasing the number of augmented plane waves in the expansion of the wave functions or increasing the number of spherical harmonics used to expand each augmented plane wave, or both. The potential function itself can be improved to include "non-muffin tin" terms.

A more fundamental method of improving accuracy is to improve the numerical methods used to solve the radial Schrödinger equation, given as

$$-\frac{1}{r^2} \frac{d}{dr} \left(r^2 \frac{d U_\ell}{dr} \right) + \left(\frac{\ell(\ell+1)}{r^2} + V(r) \right) U_\ell = E U_\ell, \quad (A.1)$$

for the radial function U_ℓ and the numerical methods used to evaluate $U'_\ell(R_S)/U_\ell(R_S)$, the logarithmic derivatives that appear in the matrix elements of the secular equation. The improvements to the methods

used in the present work will be discussed in detail in the following sections.

A.2 Starting Values

To solve the radial Schrödinger equation, Eq. (A.1), one solves for $P_{\ell}(r)$ given by

$$P_{\ell}(r) \equiv r U_{\ell}(r). \quad (\text{A.2})$$

The differential equation then becomes

$$P_{\ell}''(r) = g(r) P_{\ell}(r) \quad (\text{A.3})$$

where $P_{\ell}''(r)$ represents the second derivative of $P_{\ell}(r)$ with respect to r , and $g(r)$ is given by

$$g(r) = -E - V(r) + \frac{\ell(\ell+1)}{r^2}. \quad (\text{A.4})$$

To solve Eq. (A.3) numerically, a mesh of radial points is set up with the value of the potential $V(r_n)$ given for each point n of the mesh. The selection of this mesh is discussed in detail in Sec. A.4. The Noumerov⁴¹ method is then used to solve for $P_{\ell}(r)$ for each value of ℓ to be used. This method is used to determine the value of $P_{\ell}(r_n)$ from the value of $E, V(r_n), P_{\ell}(r_{n-1})$, and $P_{\ell}(r_{n-2})$. Therefore, to start this "outward" integration scheme of Eq. (A.3), the starting values of the radial function, $P_{\ell}(r_1)$ and $P_{\ell}(r_2)$, must be supplied. Since the accuracy of the final wave function is dependent on the accuracy of approximating these two starting values, they must be

determined with some care. Greisen⁴² has shown that the approximation

$$P_{\ell}(r_n) \simeq r_n^{\ell+1} \quad (\text{A. 5})$$

can result in errors in the eigenvalues of the APW calculation that are large compared to the self-consistency criteria; these errors are especially large for functions with a large amount of s-like symmetry. This section is devoted to the development of a more elaborate scheme of approximating these starting values, similar to those given by Hartree.⁴³

First the potential is expanded in a power series of r

$$r_n \cdot V_n = \sum_{m=0}^{\infty} b_m r_n^m \quad (\text{A. 6})$$

where

$$V_n \equiv V(r_n).$$

For small r , the expansion need be carried to only a few terms, such as

$$r_n \cdot V_n \simeq b_0 + b_1 r_n + b_2 r_n^2 \quad (\text{A. 7})$$

where

$$\lim_{r \rightarrow 0} (r_n \cdot V_n) = -2Z = b_0 \quad (\text{A. 8})$$

and where Z is the nuclear charge. To solve for the other two coefficients, Eq. (A. 7) is evaluated for $n = 1, 2$, yielding

$$r_1 \cdot V_1 \simeq -2Z + b_1 r_1 + b_2 r_1^2 \quad (\text{A. 9})$$

and

$$r_2 \cdot V_2 \simeq -2Z + b_1 r_2 + b_2 r_2^2 \quad (\text{A. 10})$$

Equations (A. 9) and (A. 10) can then be solved for b_1 and b_2 , yielding

$$b_1 = \frac{(r_2 V_1 - r_1 V_2)}{(r_2 - r_1)} + \frac{2Z(r_1 + r_2)}{r_1 r_2} \quad (\text{A. 11})$$

and

$$b_2 = \frac{(V_2 - V_1)}{(r_2 - r_1)} - \frac{2Z}{r_1 r_2} \quad (\text{A. 12})$$

Then $P_\ell(r_n)$ is expanded in a power series given by

$$P_\ell(r_n) = r_n^{\ell+1} \sum_{m=0}^{\infty} a_m r_n^m \quad (\text{A. 13})$$

where a_0 is an arbitrary constant. To approximate $P_\ell(r_1)$ and $P_\ell(r_2)$, only the first four terms of the expansion are used, yielding

$$P_\ell(r_n) \simeq a_0 r_n^{\ell+1} + a_1 r_n^{\ell+2} + a_2 r_n^{\ell+3} + a_3 r_n^{\ell+4}. \quad (\text{A. 14})$$

Substituting the expansions of $P_\ell(r_n)$ and $r_n \cdot V_n$, given in Eqs. (A. 14) and (A. 7), into the differential equation, Eq. (A. 3), the a 's can be determined by requiring that the coefficients of the power of r to vanish independently yielding

$$a_1 = - \frac{a_0 b_0}{2(\ell+1)} \quad (\text{A. 15})$$

$$a_2 = - \frac{a_0(E+b_1) + a_1 b_0}{2(2\ell+3)} \quad (\text{A. 16})$$

and

$$a_3 = - \frac{a_2 b_0 + a_0 b_2 + a_1(E+b_1)}{6(\ell+2)} \quad (\text{A. 17})$$

With these values of a_1 , a_2 , and a_3 , and setting (the so-far arbitrary) a_0 such that the value of the resulting radial function at any point never

exceeds the numerical limits of the computer, the resulting approximation to the starting values gives very accurate eigenvalues for the APW calculation.

The Nournerov method itself can be improved by a method given by Fischer,⁴⁴ but it was felt that this correction would be small compared to that resulting from the improved starting values and has not been employed in the present calculation.

A.3 Evaluation of the Derivatives at R_s

The logarithmic derivatives, P_ℓ , given by

$$D_\ell = \frac{U'_\ell(r)}{U_\ell(r)} \Big|_{r=R_s} \quad (\text{A. 18})$$

(where R_s is the radius of the APW sphere) can be evaluated using

$P'_\ell(r) \Big|_{r=R_s} \equiv P'_\ell(R_s)$ by the relationship

$$U'_\ell(R_s) = \frac{P'_\ell(R_s)}{R_s} - \frac{P_\ell(R_s)}{R_s^2} \quad (\text{A. 19})$$

The derivative of $P_\ell(R_s)$ can be evaluated very accurately if the fact is used that $P_\ell(r)$ is a solution to the differential equation

$$P''_\ell(r) = g(r) P_\ell(r)$$

given as Eq. (A.3) above.

First, the equations for $P(n+1)$ and $P(n-1)$ are given as

$$P(n+1) = P(n) + hP'(n) + \frac{h^2}{2!} P''(n) + \frac{h^3}{3!} P'''(n) + \dots \quad (\text{A. 20})$$

and

$$P(n-1) = P(n) - hP'(n) + \frac{h^2}{2!} P''(n) - \frac{h^3}{3!} P'''(n) + \dots \quad (A.21)$$

where

$$P(n) \equiv P_\ell(r_n)$$

and h is the spacing of the radial mesh points. Subtracting (A.21)

from A.20 yields

$$P(n+1) - P(n-1) = 2hP'(n) + \frac{2h^3}{3!} P'''(n) + \frac{2h^5}{5!} P^V(n) + \dots \quad (A.22)$$

Similar equation for $P(n+2)$ and $P(n-2)$ are then set up, the difference of which is given by

$$P(n+2) - P(n-2) = 4hP'(n) + \frac{16h^3}{3!} P'''(n) + \frac{64h^5}{5!} P^V(n) + \dots \quad (A.23)$$

Multiplying Eq. (A.22) by 3 and subtracting Eq. (A.23) from it yields

$$\begin{aligned} 8 \left[P(n+1) - P(n-1) \right] - \left[P(n+2) - P(n-2) \right] \\ = 12 h P'(n) - \frac{48h^5}{5!} P^V(n) + \dots \end{aligned} \quad (A.24)$$

Similarly Eq. (A.22) is multiplied by 2 and subtracted from Eq. (A.23), yielding

$$\begin{aligned} \left[P(n+2) - P(n-2) \right] - 2 \left[P(n+1) - P(n-1) \right] \\ = \frac{12h^3}{3!} P'''(n) + \frac{60h^5}{5!} P^V(n) + \dots \end{aligned} \quad (A.25)$$

Taking the second derivation of Eq. (A.25) and using the differential equation, Eq. (A.3), gives

$$\begin{aligned} \left[g(n+2)P(n+2) - g(n-2)P(n-2) \right] - 2 \left[g(n+1)P(n+1) - g(n-1)P(n-1) \right] \\ = \frac{12h^3}{3!} P^V(n) + \frac{60h^5}{5!} P^{VII}(n) + \dots \end{aligned} \quad (A.26)$$

This equation is then multiplied by $\frac{h^2}{5}$, solved for $\frac{48h^5}{5!} P^V(n)$ and substituted into Eq. (A. 24). Dropping the terms involving the seventh and higher derivatives, and solving for $P'(n)$ yields the final relationship given by

$$P'(n) = \frac{1}{12h} \left\{ \left[1 - \frac{h^2}{5} g(n-2) \right] P(n-2) - \left[8 - \frac{2h^2}{5} g(n-1) \right] P(n-1) + \left[8 - \frac{2h^2}{5} g(n+1) \right] P(n+1) - \left[1 - \frac{h^2}{5} g(n+2) \right] P(n+2) \right\} \quad (A. 27)$$

which was used in Eq. (A. 19) to evaluate the logarithmic derivatives in these calculations.

A. 4 Effects of the Choice of Radial Mesh

In the application of numerical methods to the solution of the radial Schrödinger equation, Eq. (A. 3), a radial mesh must be set up for a finite number of points, usually between 100 and 1000 points. The spacing of the radial points must be small at small values of the radius (r) to insure accurate results in the region where both the potential function and the wave function are varying rapidly. The spacing must then be increased (if we are to keep the total number of points within reason) as r increases so that the mesh will cover the range of r required for the calculation.

There are essentially two ways of defining such a radial mesh. The first, known as the logarithmic mesh, is given by

$$r_n = R_0 e^{nh} \quad (A. 28)$$

where R_0 and h are set to satisfy the spacing and range requirements

of the mesh, as mentioned above. The main advantage of this type mesh is its simplicity. However, as will be shown later, this is also the main disadvantage. The second, called a linear mesh, is set up in blocks of mesh points, in which the mesh spacing is constant between each mesh point. In this type of mesh, the spacing is set up to be small in the first block and is doubled as r goes into each succeeding block. These blocks, usually less than 10 in number, need not contain the same number of points and can be adjusted so that the range of r values required is covered while retaining some control of the spacing at the extremes of r . This versatility is the main advantage of the linear mesh and the lack of it, the main disadvantage of the logarithmic mesh.

To test the accuracy that can be achieved when solving the radial Schrödinger equation numerically for these two types of radial meshes, the logarithmic derivatives evaluated at R_g were determined for a pure coulombic potential $-2Z/r$ by both numerical and analytical methods. These results are tabulated and the compared for the two radial meshes considered. Tests on the accuracy of evaluating the eigenvalues of the core states on a linear mesh are also presented.

The logarithmic derivatives for 16 different logarithmic radial meshes are given in Table (A.1) for $\ell = 0, 1$, and 2 . The energy was set at 0.1 Ry , which is representative of the energy-band states. The values of $Z=26$ and $R_g=2.5 \text{ a.u.}$ were selected so that a comparison

TABLE A. 1

The logarithmic derivatives U'_ℓ/U_ℓ , evaluated at $R_s = 2.5$, for a $-2Z/r$ potential, with $Z = 26$, on a logarithmic radial mesh. The energy in all cases was 0.1 Ry. R_1 is the minimum r value used and N is the total number of radial mesh points.

R_1 (a. u.)	N	ΔR @ R_s	U'_ℓ/U_ℓ		
			$(\ell=0) \times 10^{-2}$	$(\ell=1) \times 10^{-2}$	$(\ell=2) \times 10^{-1}$
10^{-2}	200	0.071	4.59011	1.15084	3.96734
10^{-2}	300	0.047	4.59583	1.15117	3.96782
10^{-2}	400	0.035	4.59684	1.15123	3.96790
10^{-2}	500	0.028	4.59716	1.15124	3.96792
10^{-4}	200	0.132	4.53063	1.14639	3.96066
10^{-4}	300	0.087	4.59258	1.15033	3.96662
10^{-4}	400	0.065	4.60286	1.15097	3.96753
10^{-4}	500	0.051	4.60563*	1.15114*	3.96777*
10^{-6}	200	0.194	4.27631	1.12869	3.93144
10^{-6}	300	0.127	4.54079	1.14705	3.96168
10^{-6}	400	0.095	4.58566	1.14996	3.96607
10^{-6}	500	0.075	4.59900	1.15073	3.96719
10^{-8}	200	0.258	3.72558	1.08247	3.84538
10^{-8}	300	0.168	4.41285	1.13847	3.94797
10^{-8}	400	0.125	4.54544	1.14735	3.96214
10^{-8}	500	0.099	4.58218	1.14968	3.96566

*Value nearest analytic results.

could be made with analytical results made available by Wood.⁴⁵ The results of this table are displayed graphically in Figs. (A. 1), (A. 2), and (A. 3). The main feature of interest, which shows up especially well in Fig. (A. 1), is that $R_1 \leq 10^{-4}$ a.u., the accuracy of the logarithmic derivatives is dependent almost entirely on the mesh spacing at R_g . This is also true in Figs. (A. 2) and (A. 3), but it is not as obvious. This does show up in Table (A. 1) in all three cases, where the most accurate values of the logarithmic derivatives are achieved with 500 points and $R_1 = 10^{-4}$. The relative errors for these three results are 0.0004, 0.0001, and 0.00004 for $\ell = 0, 1$, and 2, respectively.

The relative errors in the logarithmic derivatives, evaluated for $\ell = 0, 1$, and 2, on four linear meshes are given in Table (A. 2), and the relative errors in the eigenvalues of the "core" states are given in Table (A. 3) for the same four linear meshes. It should be pointed out that not only is $R_1 \simeq 10^{-4}$ in all four cases, but the spacing is so constructed as to maintain a smaller spacing at R_g than can be achieved with the logarithmic mesh.

Comparing the results for a 200 point linear mesh with the results for the "best" 500 point logarithmic mesh, the relative error is one tenth as large for the linear mesh. It can easily be understood why the linear mesh was selected for use in the present calculations.

Figure A.1. The $\ell = 0$ logarithmic derivatives for a $-2Z/r$ potential as a function of the logarithmic mesh. Data plotted from Table (A.1).

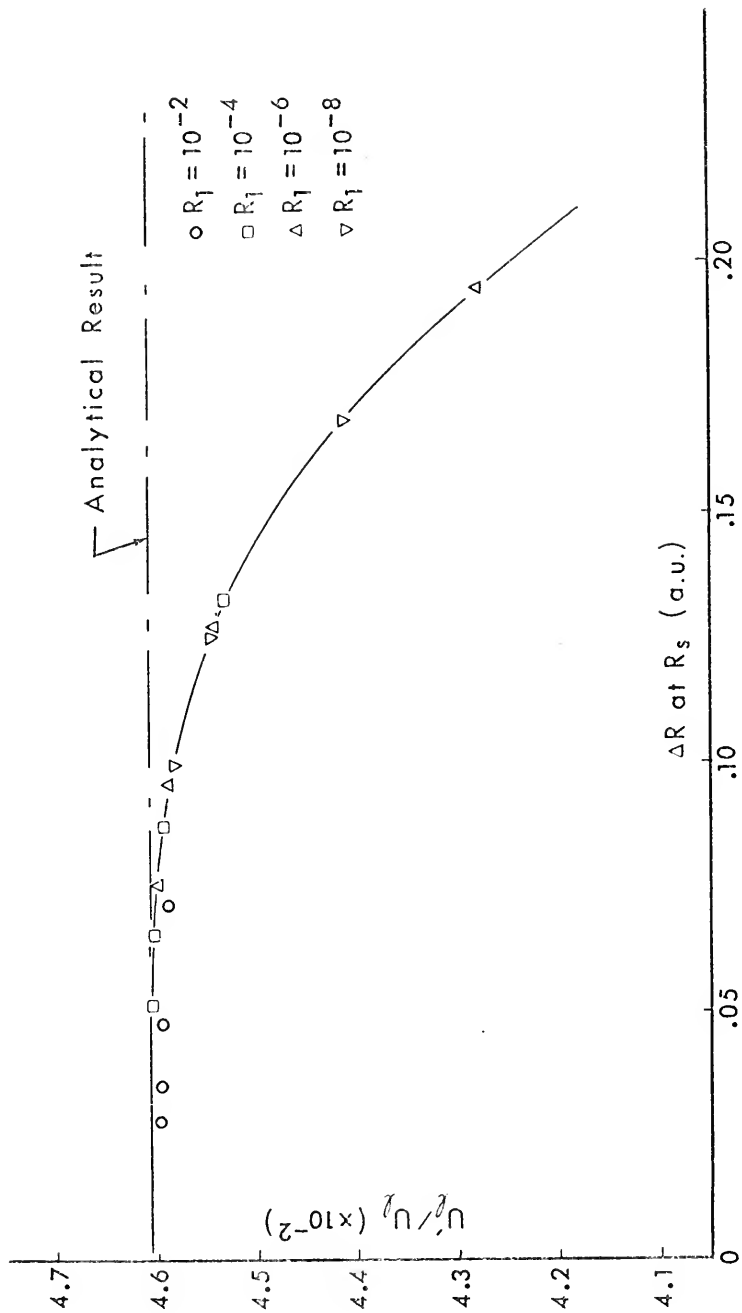


Figure A.1

Figure A.2. The $\ell = 1$ logarithmic derivatives for a $-2Z/r$ potential as a function of the logarithmic mesh. Data plotted from Table (A.1).

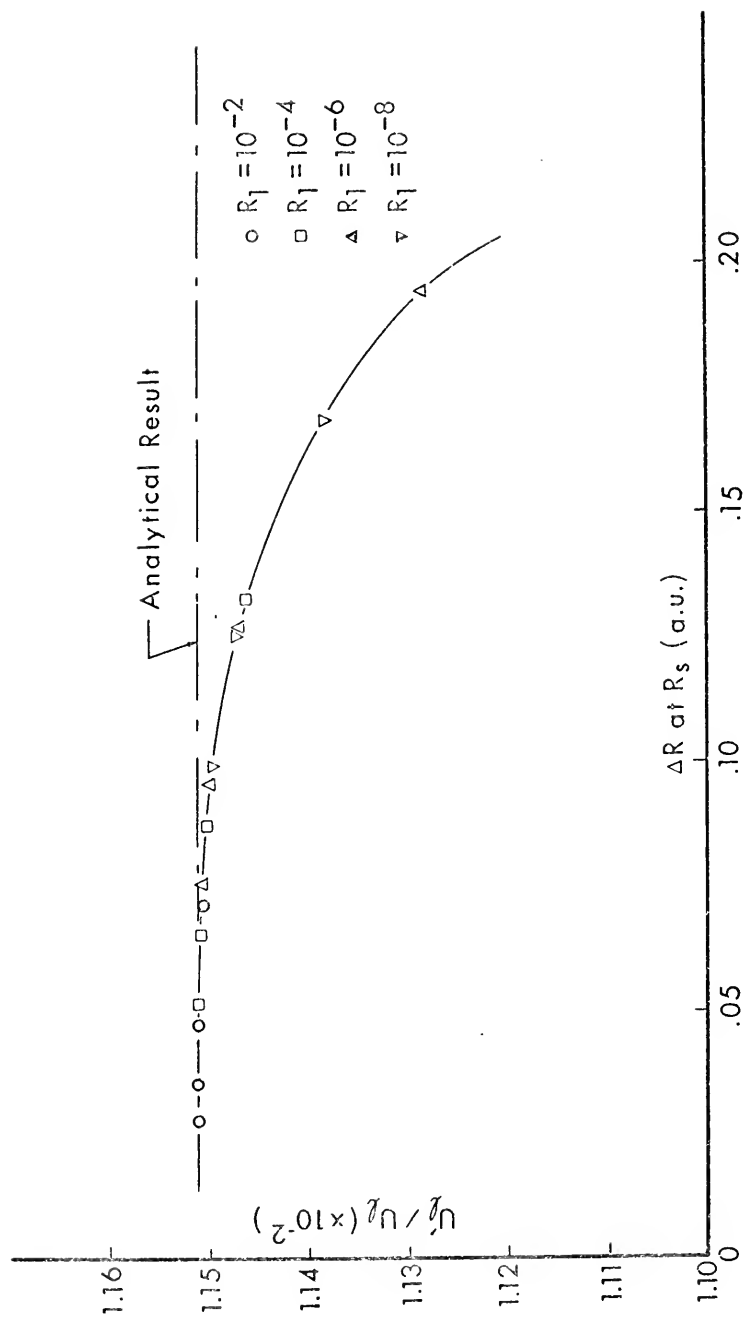


Figure A.2

Figure A.3. The $\ell = 2$ logarithmic derivatives for a $-2Z/r$ potential as a function of the logarithmic mesh. Data plotted from Table (A.1).

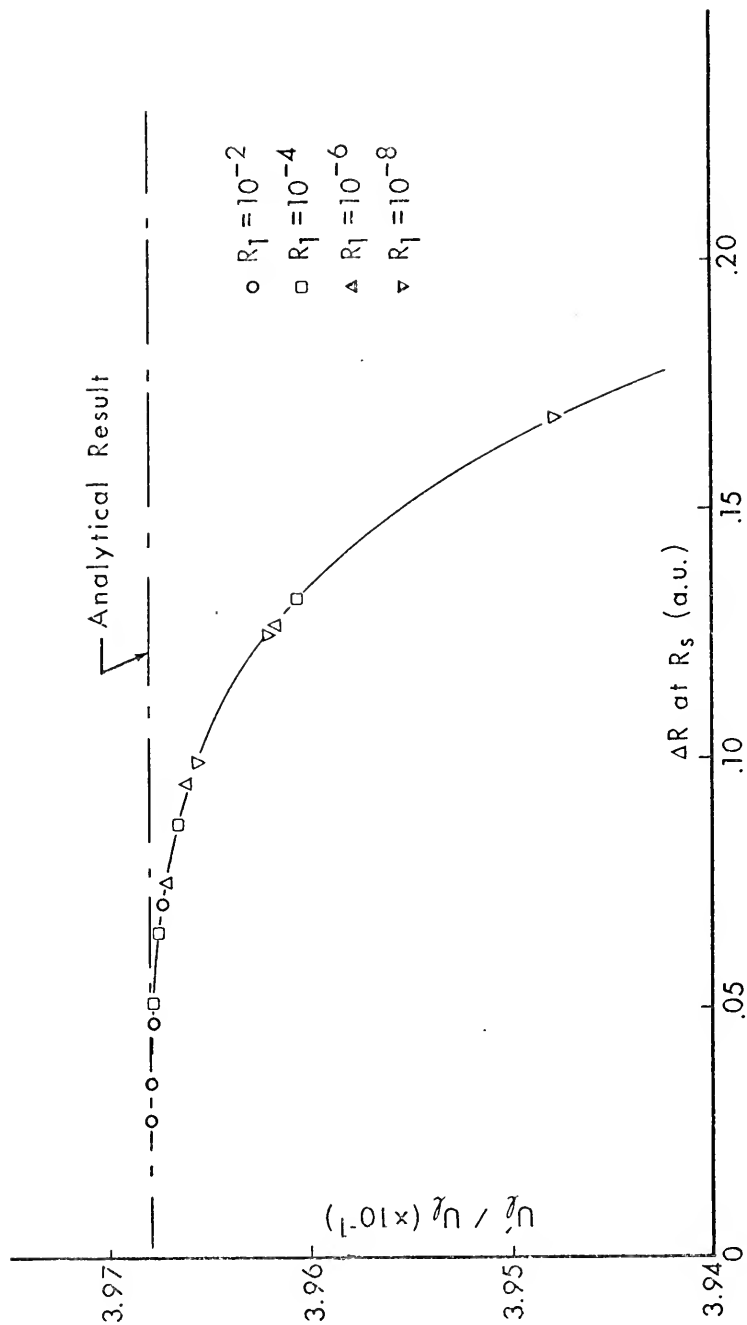


Figure A.3

TABLE A.2

The relative error in the logarithmic derivatives for four linear radial meshes, with $R_S = 2.5$ a.u., $Z = 26$ a.u., and $E = 0.10$ Ry, for a $-2Z/r$ test potential. R_1 is the minimum value of r used and N is the total number of points in the radial mesh.

N	$R_1 \times 10^4$ (a.u.)	ΔR @ R_S	Relative error in U'_ℓ / U_ℓ		
			$\ell = 0$	$\ell = 1$	$\ell = 2$
200	2.6	0.017	6.5×10^{-5}	1.4×10^{-5}	1.1×10^{-5}
300	2.1	0.013	8.2×10^{-6}	3.5×10^{-6}	2.1×10^{-6}
400	1.7	0.011	5.3×10^{-6}	1.5×10^{-6}	7.0×10^{-7}
500	1.4	0.009	2.9×10^{-6}	7.0×10^{-7}	3.0×10^{-7}

TABLE A.3

Relative error in the core state eigenvalues for four linear meshes, with $R_S = 2.5$ a.u., $Z = 26$ a.u., and a $-2Z/r$ test potential. R_1 is the minimum value of r used and N is the total number of points in the radial mesh.

	N=200 $R_1 = 2.6 \times 10^{-4}$ $\Delta R_{R_S} = 0.017$	N=300 $R_1 = 2.1 \times 10^{-4}$ $\Delta R_{R_S} = 0.013$	N=400 $R_1 = 1.7 \times 10^{-4}$ $\Delta R_{R_S} = 0.011$	N=500 $R_1 = 1.4 \times 10^{-4}$ $\Delta R_{R_S} = 0.009$
1s	2.4×10^{-6}	3.9×10^{-7}	9.9×10^{-8}	2.1×10^{-8}
2s	1.8×10^{-6}	1.7×10^{-7}	2.9×10^{-8}	1.3×10^{-8}
2p	1.0×10^{-6}	1.1×10^{-7}	2.2×10^{-8}	1.0×10^{-8}
3s*	1.8×10^{-6}	4.1×10^{-6}	1.8×10^{-6}	6.9×10^{-7}
3p*	1.5×10^{-6}	2.6×10^{-6}	1.2×10^{-6}	5.2×10^{-7}

*These states are considered as band states in the present calculations.

APPENDIX B

TOTAL ENERGY CALCULATIONS USED TO EVALUATE THE "FROZEN CORE" MODEL

The "frozen core" model of a self-consistent APW calculation is based on the assumption that the core state functions do not change much while going from the free atom to the self-consistent crystal result, and can, therefore, be held fixed throughout the calculation without significantly affecting the results. Some insight into the validity of this assumption can be obtained if the total energy is broken up such that

$$E = E_{c-c} + E_{v-v} + E_{c-v} \quad (B.1)$$

where E_{c-c} is that part of the total energy resulting from the kinetic energy of the core electrons and that part of the potential energy representing the coulomb and exchange interactions of the core electrons with the nucleus and the other core electrons. E_{v-v} represents the same energy for the valence electrons, and E_{c-v} represents the interactions between the core and valence electrons. The E_{c-c} energies for the self-consistent crystal calculations and the free atom calculation can be determined and compared, giving an indication as to how these core states vary, and as to what effect these variations might have on total energy calculations.

To evaluate these energies, the total charge density is divided into that associated with the core states, $\rho_c(r)$, and that associated with the valence state, $\rho_v(r)$, such that

$$\rho(r) = \rho_c(r) + \rho_v(r). \quad (B.2)$$

The total core-core energy, E_{c-c} , is then given by

$$E_{c-c} = \sum_c \nabla_1^2 + \frac{1}{2} \int_{\text{cell}} V_c(r) \cdot \rho_c(r) dr + \int_{\text{cell}} W_c(r) \cdot \rho_c(r) dr + \frac{Z}{2} V_{0c} \quad (B.3)$$

where

$$V_c(r) = -\frac{2Z}{r} + \frac{2}{r} \int_0^r \rho_c(r') dr' - 2 \int_r^{R_s} \frac{\rho_c(r')}{r'} dr' + C \quad (B.4)$$

$$W_c(r) = -\frac{3}{2} \alpha \left(\frac{81}{4\pi^2} \right)^{\frac{1}{3}} \left(\frac{\rho_c(r)}{r^2} \right)^{\frac{1}{3}} \quad (B.5)$$

$$V_{0c} = -2 \int_0^{R_s} \frac{\rho_c(r')}{r'} dr' + C \quad (B.6)$$

and $\sum_c \nabla_1^2$ is the total kinetic energy of the core electrons. The total valence-valence energy, E_{v-v} , is given by the same four equations with the subscript (c) replaced by the subscript (v). The energy associated with the core-valence interactions is given by

$$E_{c-v} = E - (E_{c-c} + E_{v-v}). \quad (B.7)$$

The results for a calculation on copper with $\alpha = 0.7225$, and two core configurations are given in Table (B.1). The most interesting results are the differences in core-core energies for the two configurations. If the configuration of the "frozen core" was selected to be $1s^2 2s^2 2p^6$, (1s-2p), the difference of the core-core energy would

TABLE B. 1

Total energies for self-consistent atomic and crystal calculations on copper with $\alpha = 0.7225$, for two core configurations.

	Energy (Ry)		
	Crystal	Atomic	Difference
(1s-3p) Core			
Core-Core	-3177.7552	-3177.5900	0.1653
Val. - Val.	- 552.4849	- 550.5609	1.9240
Core-Val.	449.1419	447.3383	-1.8036
(1s-2p) Core			
Core-Core	-2885.6566	-2885.6624	-0.0058
Val. - Val.	- 938.8640	- 937.3516	1.5124
Core-Val.	543.4224	542.2015	-1.2209
Total	-3281.0932	-3280.8125	0.2857*

*Cohesive energy.

indicate that this should be an acceptable model. However, if the configuration is chosen to be $1s^2 2s^2 2p^6 3s^2 3p^6$, (1s-3p), which is usually done, the difference in core-core energy is on the order of the cohesive energy which indicates changes in some of these core states, namely the 3s and 3p states, that could have significant effects on such quantities as cohesive energy or pressure, and the use of such a "frozen core" model would be somewhat limited.

APPENDIX C

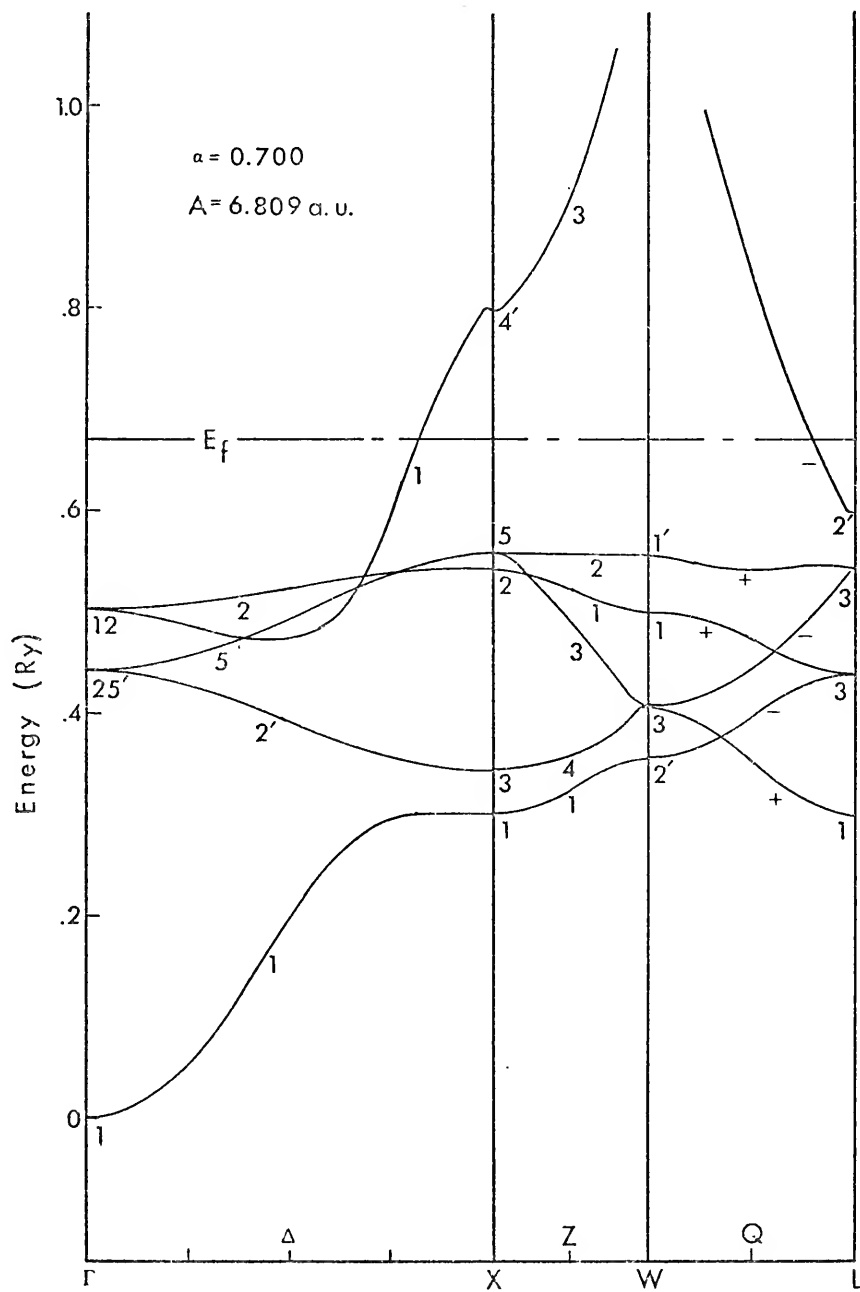
THE ENERGY BANDS, DENSITY OF STATES, TOTAL ENERGY, AND COHESIVE ENERGY OF COPPER AS A FUNCTION OF α

C.1 The Energy Bands and Density of States

This section is devoted to the presentation of the energy bands and density of states for the four values of α used to determine the α that yields zero pressure at the observed lattice spacing, as described in Sec. 3.1. Each calculation was done for 2048 points in the first Brillouin zone and used a 500 point linear radial mesh (for integration of the radial Schrödinger equation). Though the self-consistency criterion used in these calculations was applied to the pressure variation between two successive iterations, the variation of any eigenvalue between two successive iterations was found to be less than 10^{-4} Ry for the core states (usually the 1s state has the largest variation) and less than 10^{-5} Ry for the band states. The resulting change in total energy between two successive iterations was about 10^{-6} Ry.

Figures C.1, C.2, C.3, and C.4 show the energy bands for copper for four values of α , along the directions of highest symmetry in the first Brillouin zone. All four correspond to an APW sphere radius (R_s) of 2.407 a.u., which is one half the nearest neighbor distance for the experimentally determined lattice spacing extrapolated

Figure C.1. (a&b) Energy bands for FCC copper with $\alpha = 0.700$ and $R_g = 2.407$ a.u. (c) Density of states for this calculation.



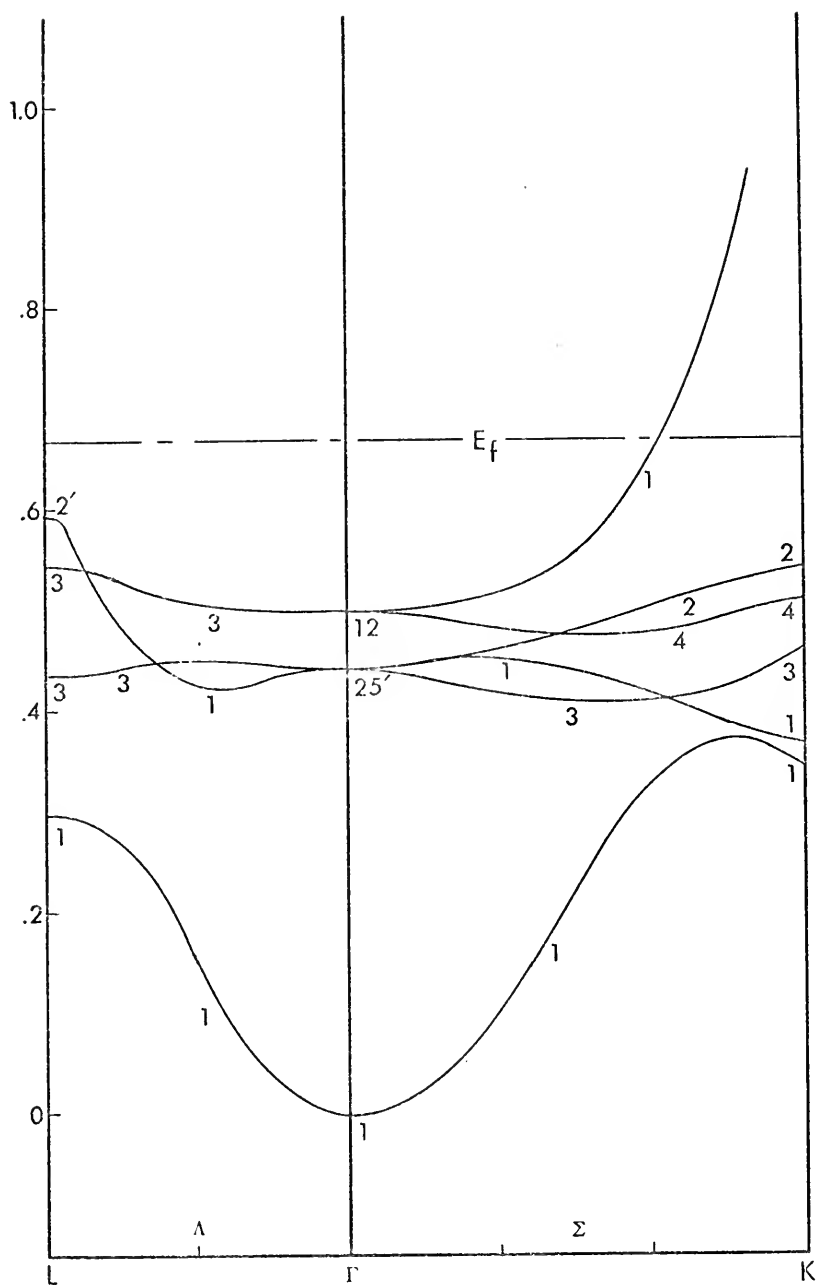


Figure C.1b

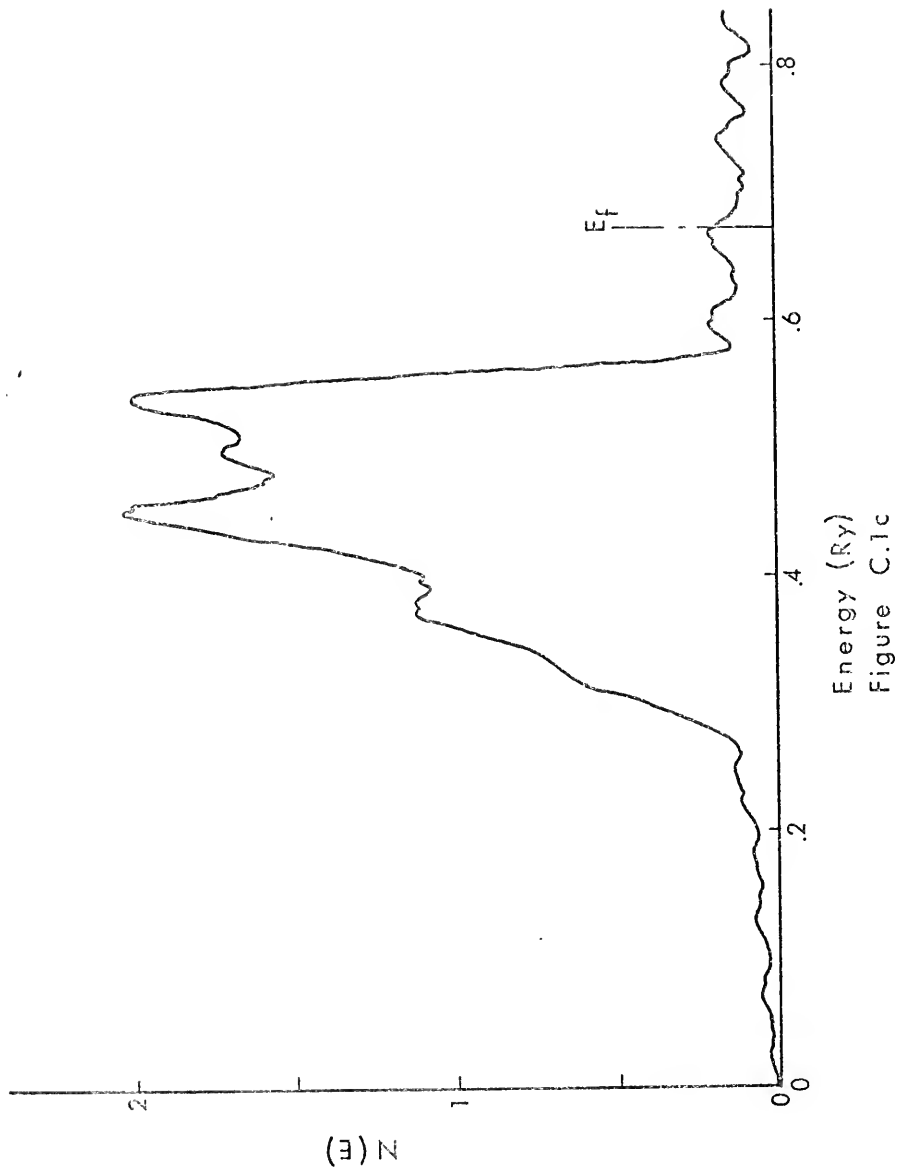


Figure C.2. (a&b) Energy bands for FCC copper with $\alpha = 0.70635$ and $R_S = 2.407$ a.u. (c) Density of states for this calculation.

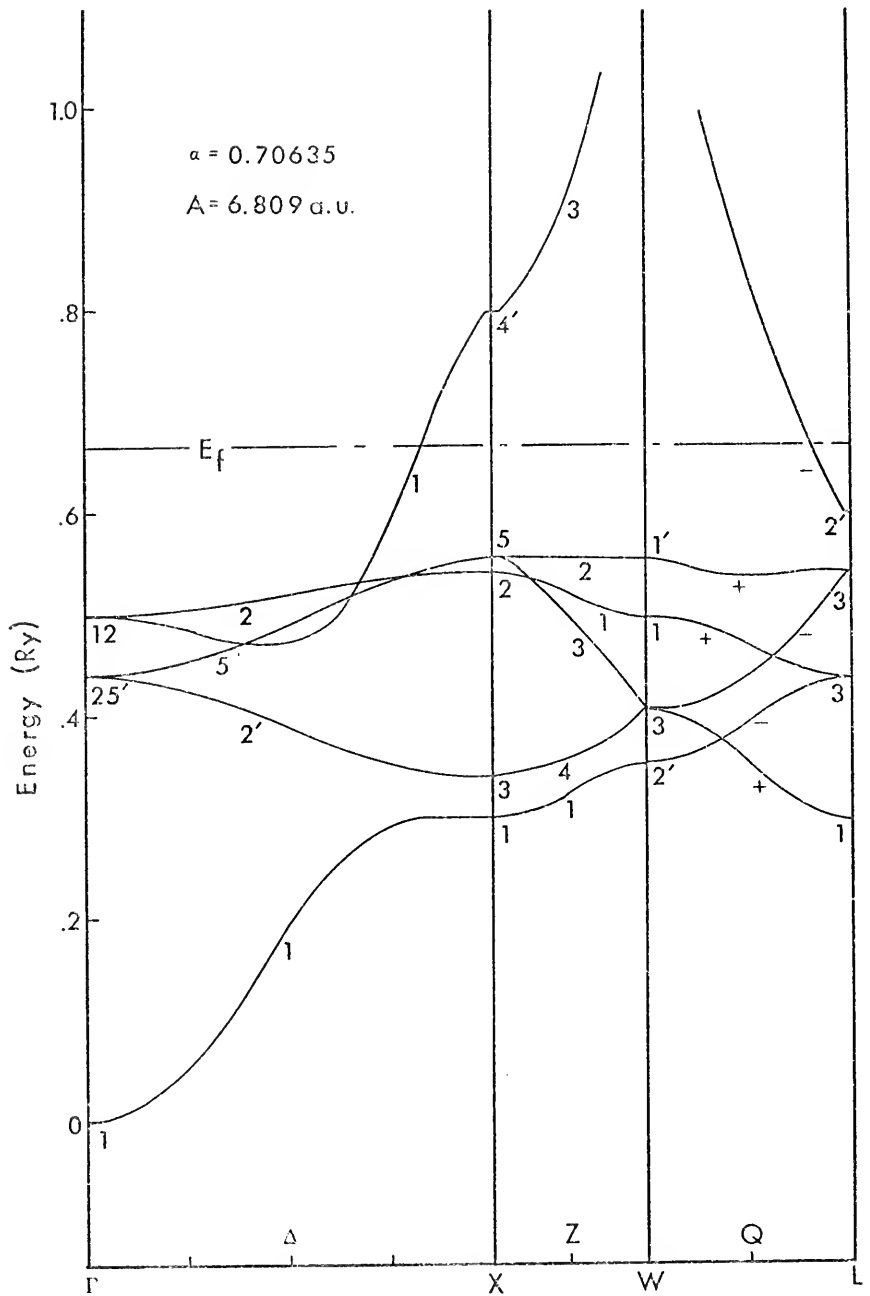


Figure C.2a

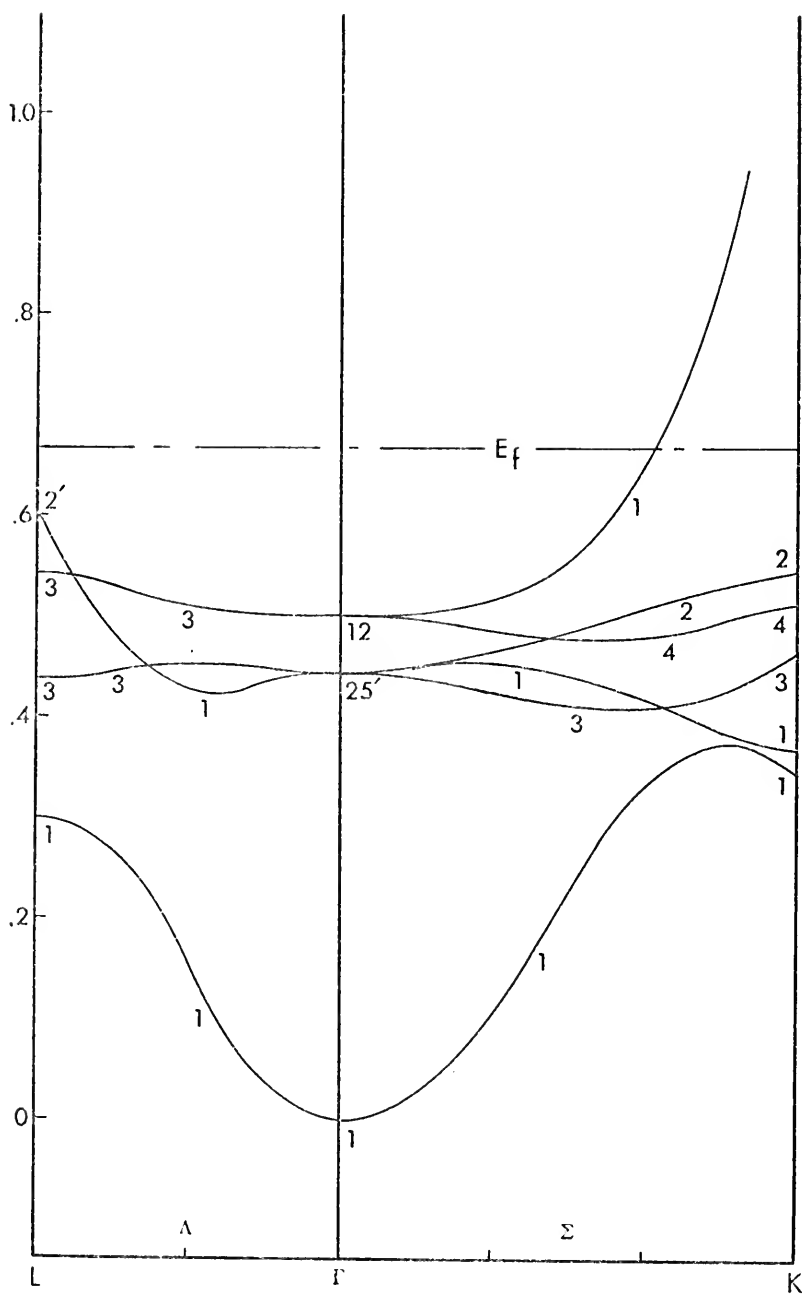


Figure C.2b

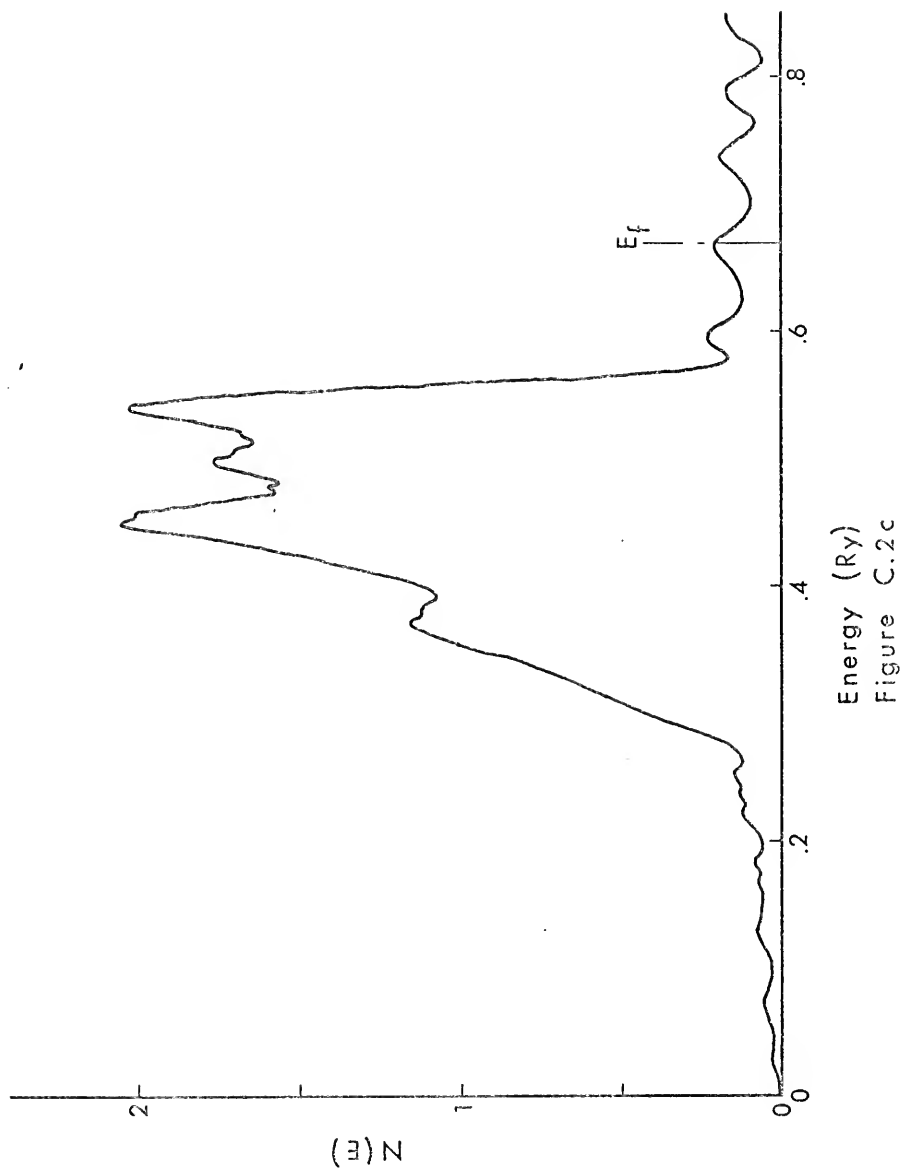


Figure C.2c

Figure C.3. (a&b) Energy bands for FCC copper with $\alpha = 0.720$ and $R_s = 2.407$ a.u. (c) Density of states for this calculation.

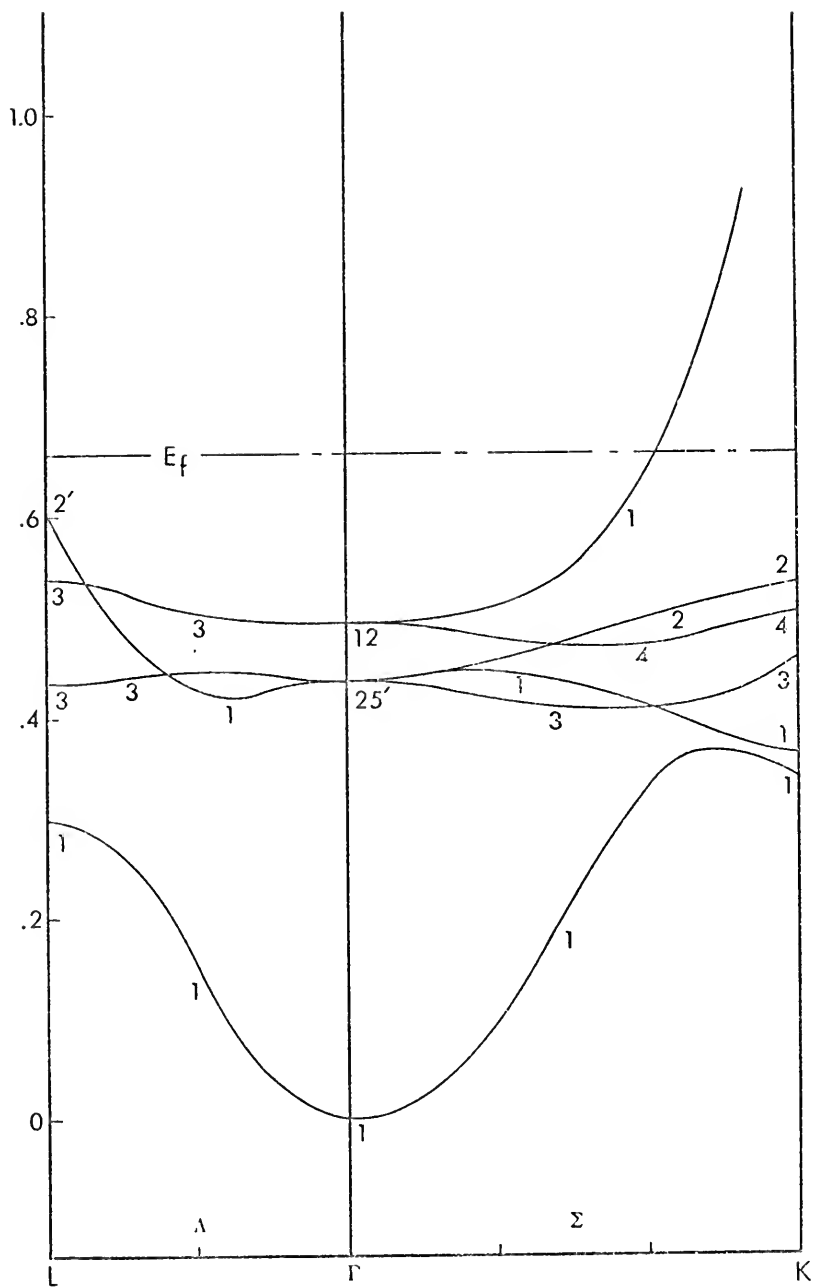


Figure C.3b

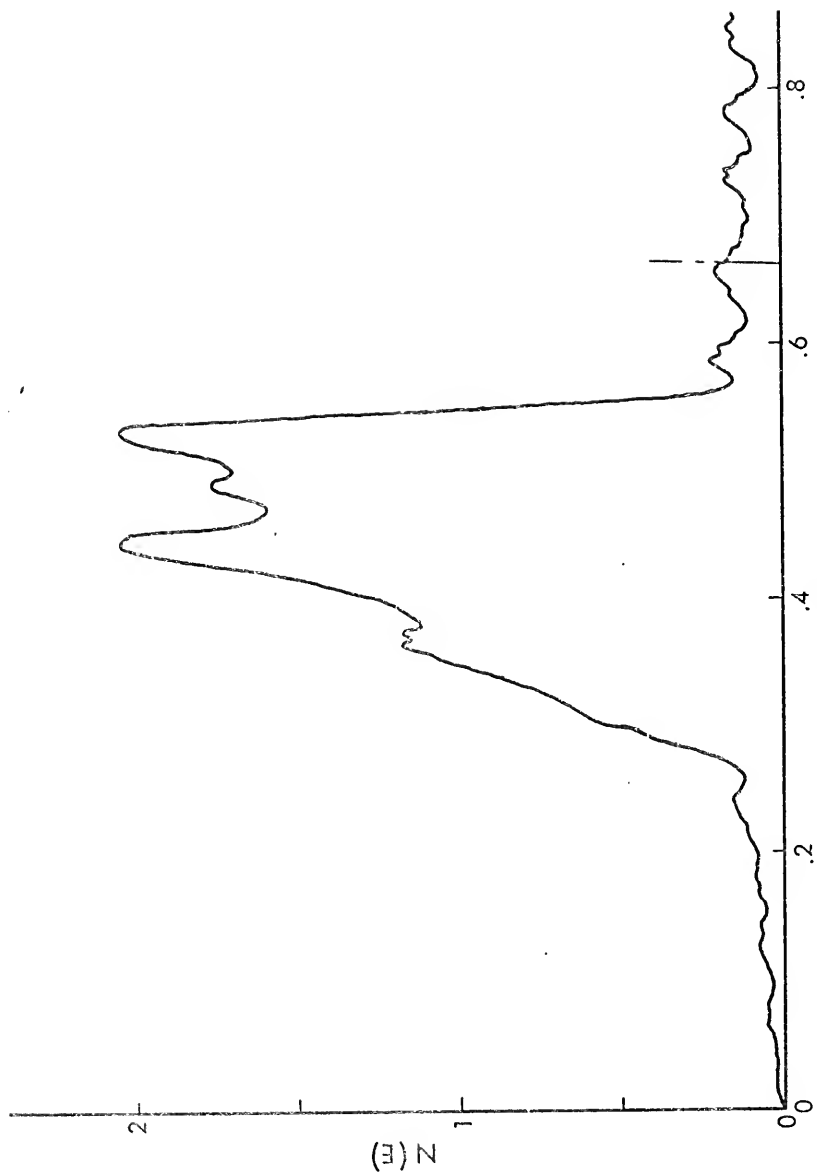


Figure C.3c

Figure C.4. (a&b) Energy bands for FCC copper with $\alpha = 0.770$ and $R_s = 2.407$ a.u. (c) Density of states for this calculation.

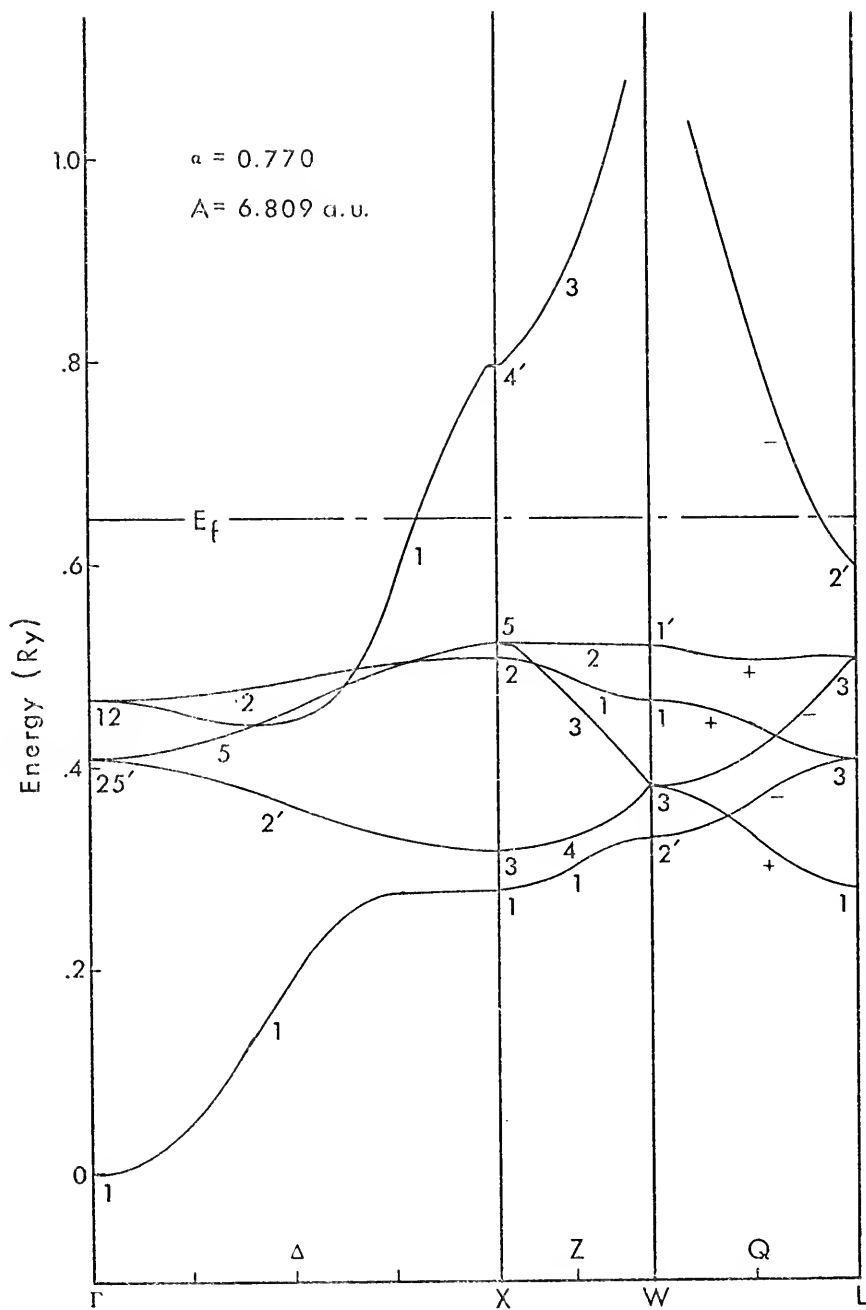


Figure C.4a

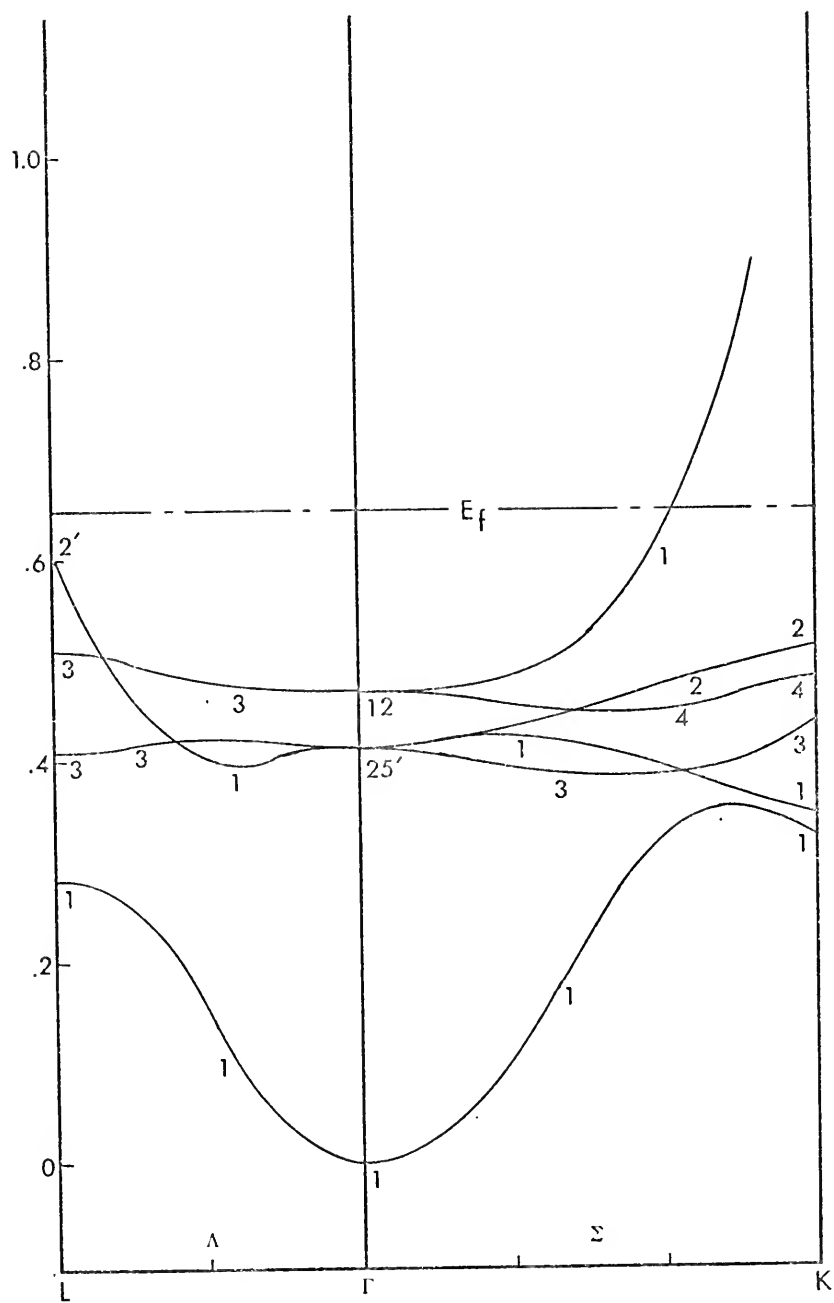
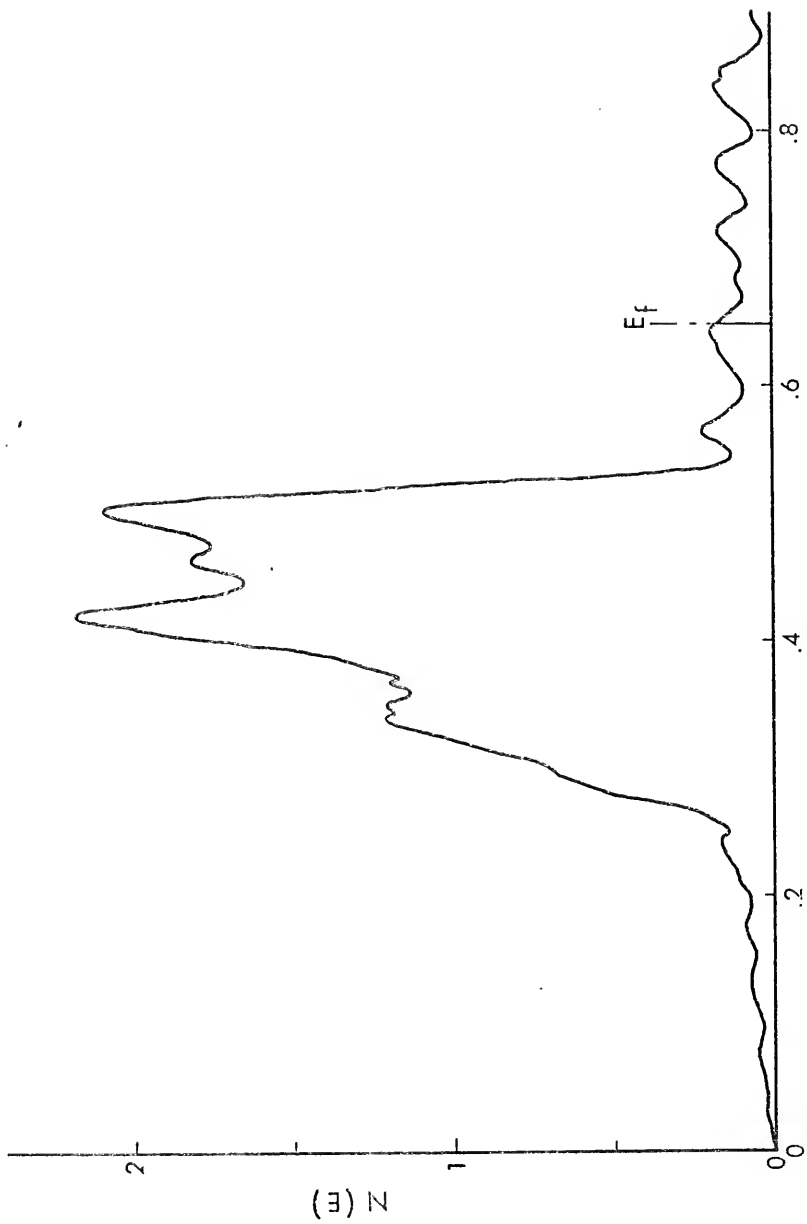


Figure C.4b



Energy (Ry)
Figure C.4c

to 0°K. The corresponding density of states for each calculation is also given.

Table C.1 gives energy differences for these calculations, that represent the bandwidths and relative locations of the bands with respect to each other and with respect to the Fermi energy. The energy differences $(\Gamma_{25'} - \Gamma_1)$ and $(X_5 - \Gamma_1)$ give the relative location of the d-band with respect to the sp-band, while the differences $(E_f - X_5)$ and $(E_f - L_3)$ locate the top of the d-band with respect to the Fermi energy. The energy differences $(X_5 - X_1)$ and $(X_{4'} - \Gamma_1)$ give the bandwidths of the d-band and sp-band respectively. $(E_f - L_{2'})$ represents the location of the high symmetry point with an eigenvalue nearest the Fermi energy. This energy difference gives an indication of the "neck" radius of the copper Fermi surface; the necks lie along the $[111]$ directions.

Also included in the table are energy differences resulting from the calculation for $\alpha = 0.7225$, using the experimentally determined lattice parameter, and a similar calculation for $\alpha = 2/3$. (This latter calculation was carried to a convergence of only 10^{-3} Ry for the total energy.) Results of previous calculations and experiment are also included for comparison.

The variation of the relative locations and widths of the bands as a function of α are as found in previous calculations. That is, as α is increased, the d-band narrows and its average energy moves closer to the bottom of the sp-band at Γ_1 , while the sp-band width

TABLE C.1.

Energy differences for states that indicate positions and widths of sp-band and d-band (Ry).

	$\Gamma_2'-\Gamma_1$	$X_5-\Gamma_1$	X_5-X_1	$X_4'-\Gamma_1$	E_f-X_5	E_f-L_3	E_f-L_2'
			Experimental				
Spicer ^a			0.250		0.147		0.026
Lettington ^b					0.147	0.162	
Eastman ^c			0.220				
Lindau & Wallden ^d							
			Previous calculations (not self-consistent)				0.055
Segall ^e	0.331	0.470	0.300	0.307	0.183	0.197	0.064
Burdick ^f	0.399	0.512	0.249	0.804	0.143	0.154	0.045
Mattheiss ^g	0.463	0.570	0.252	0.794			
Faulkner et al. ^h							
V _I				0.808			0.056
V _{II}				0.799			0.089
V _{VIII}				0.804			-0.019
			Previous calculations (self-consistent)				
Wakoh ⁱ	0.386	0.499	0.245		0.159		
Snow ^j							
$\alpha = 1$	0.278	0.369	0.189	0.793	0.223	0.232	-0.005
$\alpha = 5/6$	0.375	0.477	0.224	0.794	0.149	0.159	0.029
Janak et al. ^k							
Hedin-Lundqvist	0.454	0.578	0.260	0.796	0.112		0.082
$\alpha = 0.706$	0.447	0.560	0.256	0.796	0.116		0.078
$\alpha = 0.721$	0.438	0.550	0.252	0.796	0.122		0.074
$\alpha = 0.770$	0.417	0.525	0.242	0.795	0.133		0.061
$\alpha = 0.833$	0.385	0.490	0.229	0.794	0.153		0.045

--Continued--

TABLE C. 1 Continued

	$\Gamma_{25}^{'-}\Gamma_1$	$X_5^{'-}\Gamma_1$	$X_5^{'-}X_1$	$X_4^{'-}\Gamma_1$	$E_f^{'-}X_5$	$E_f^{'-}L_3$	$E_f^{'-}L_2$
$\alpha = 0.66667$	0.460	0.578	0.264	0.802	0.102	0.116	0.080
$\alpha = 0.70000$	0.445	0.561	0.257	0.801	0.109	0.122	0.070
$\alpha = 0.70635$	0.442	0.558	0.256	0.801	0.110	0.124	0.068
$\alpha = 0.72000$	0.436	0.551	0.253	0.801	0.113	0.127	0.063
$\alpha = 0.72250$	0.435	0.549	0.252	0.801	0.114	0.127	0.063
$\alpha = 0.77000$	0.413	0.523	0.242	0.801	0.125	0.139	0.049

a Reference 36

b Reference 37

c Reference 38

d Reference 39

e Reference 46

f Reference 47

g Reference 48

h Reference 49

i Reference 50

j Reference 6

k Reference 40

remains relatively unaffected. The Fermi energy follows the movement and the d-band, moving toward Γ_1 as α increases.

The bandwidths and relative locations for the present calculations are in good agreement with those determined recently by Janak et al.⁴⁰ using the KKR method. The only significant differences are the locations of the X_5 and L_2' eigenvalues with respect to the Fermi energy. However, these discrepancies can probably be attributed to the accuracies of the different approaches to locating the Fermi energy in the two different methods. Part of these discrepancies could probably be eliminated if a weighting scheme for states with eigenvalues near the Fermi energy, similar to that used by Hattox,²⁸ were used for locating the Fermi energy in the present calculations.

C.2 Total Energy and Cohesive Energy as a Function of α for Copper ($A=A_0$)

The total energy and cohesive energy for the six calculations, listed as present calculations in Table C.1, are given in Table C.2. Also included in the table are the relative differences between the calculated values of cohesive energy and the experimentally determined value of 0.257 Ry.³⁴ The total energy as a function of α is plotted in Figs. C.5 and C.6 for these six solid calculations and for six atomic calculations respectively. Figure C.7 is a plot of the cohesive energy as a function of α for the same solid calculations.

As was pointed out in Sec. 3.1, the total energy for both solid and atomic calculations is very nearly a linear function of α . However, the nonlinearity of the cohesive energy indicates that the linear

TABLE C.2

Total energy and cohesive energy as a function of α for copper ($A=A_0$).

α	Metal (Ry)	Atom (Ry)	Cohesive Energy (Ry)	Relative difference from experimental cohesive energy. *
0.66667	-3270.7237	-3270.4534	0.2703	0.05
0.70000	-3276.9131	-3276.6333	0.2798	0.09
0.70635	-3278.0937	-3277.8122	0.2814	0.09
0.72000	-3280.6330	-3280.3480	0.2850	0.11
0.72250	-3281.0982	-3280.8126	0.2857	0.11
0.77000	-3289.9519	-3289.6552	0.2967	0.15

*Experimental value of cohesive energy is 0.257 Ry.³⁴

Figure C.5. Total energy as a function of the parameter α , for metallic copper ($A=A_0$).

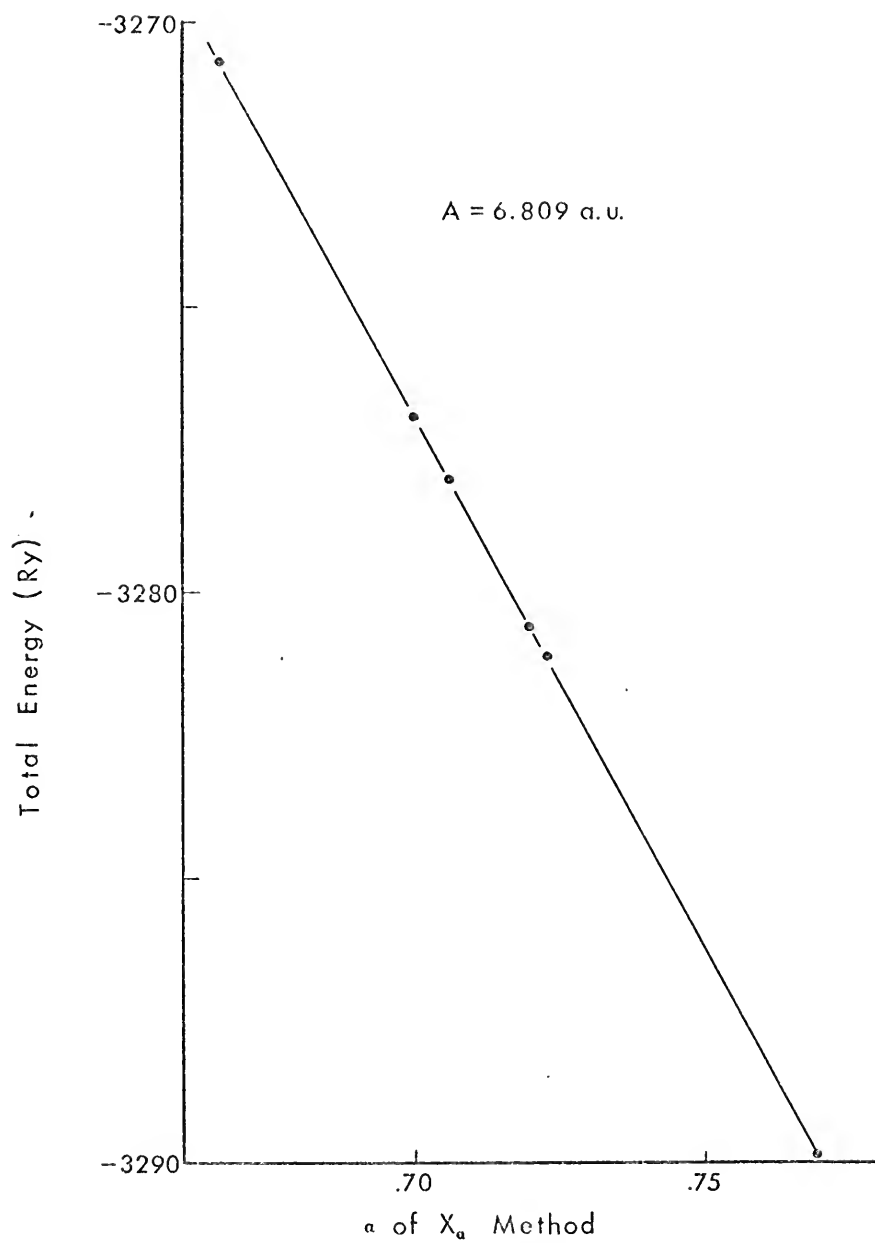


Figure C.5

Figure C.6. Total energy as a function of the parameter α , for atomic copper.

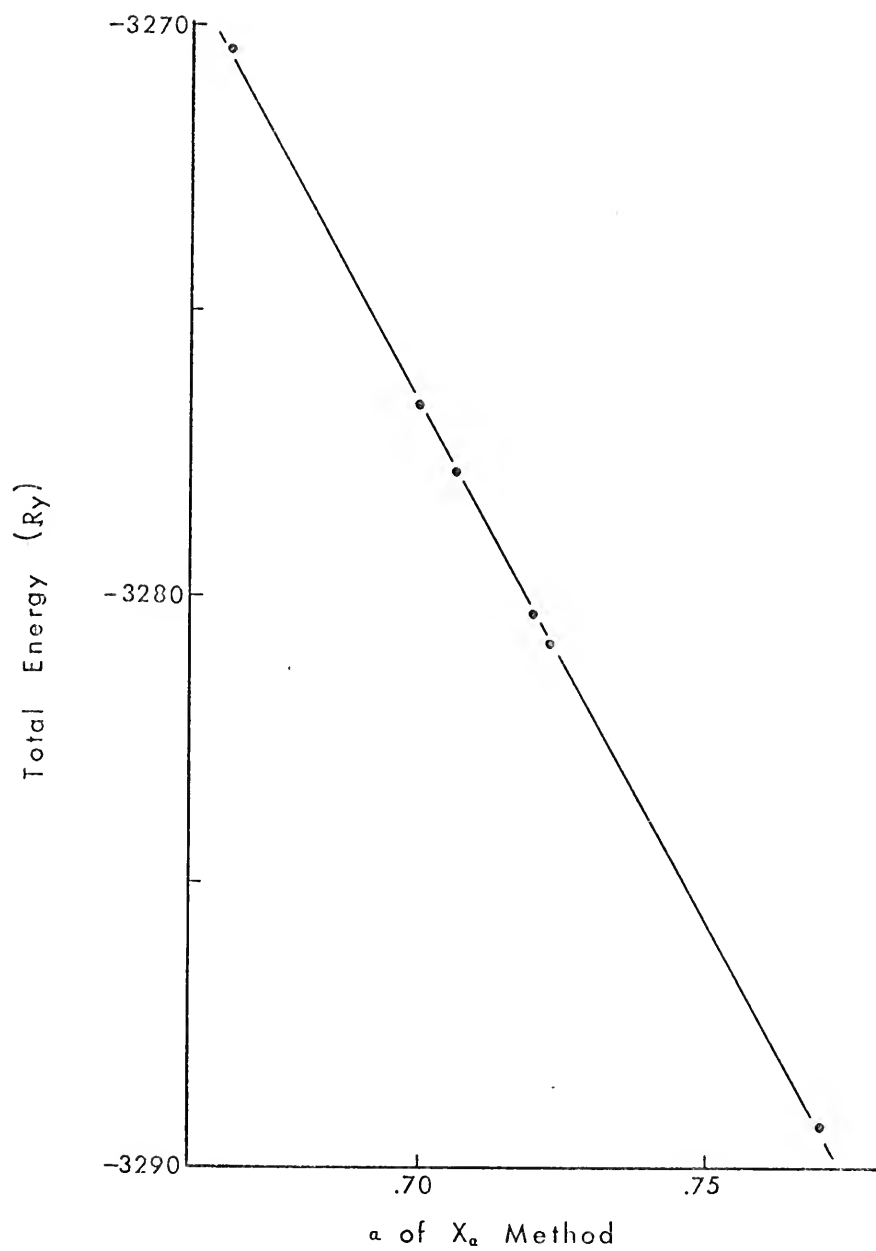


Figure C.6

Figure C.7. The cohesive energy of copper as a function of the parameter α of the $N\alpha$ method ($A=A_0$).

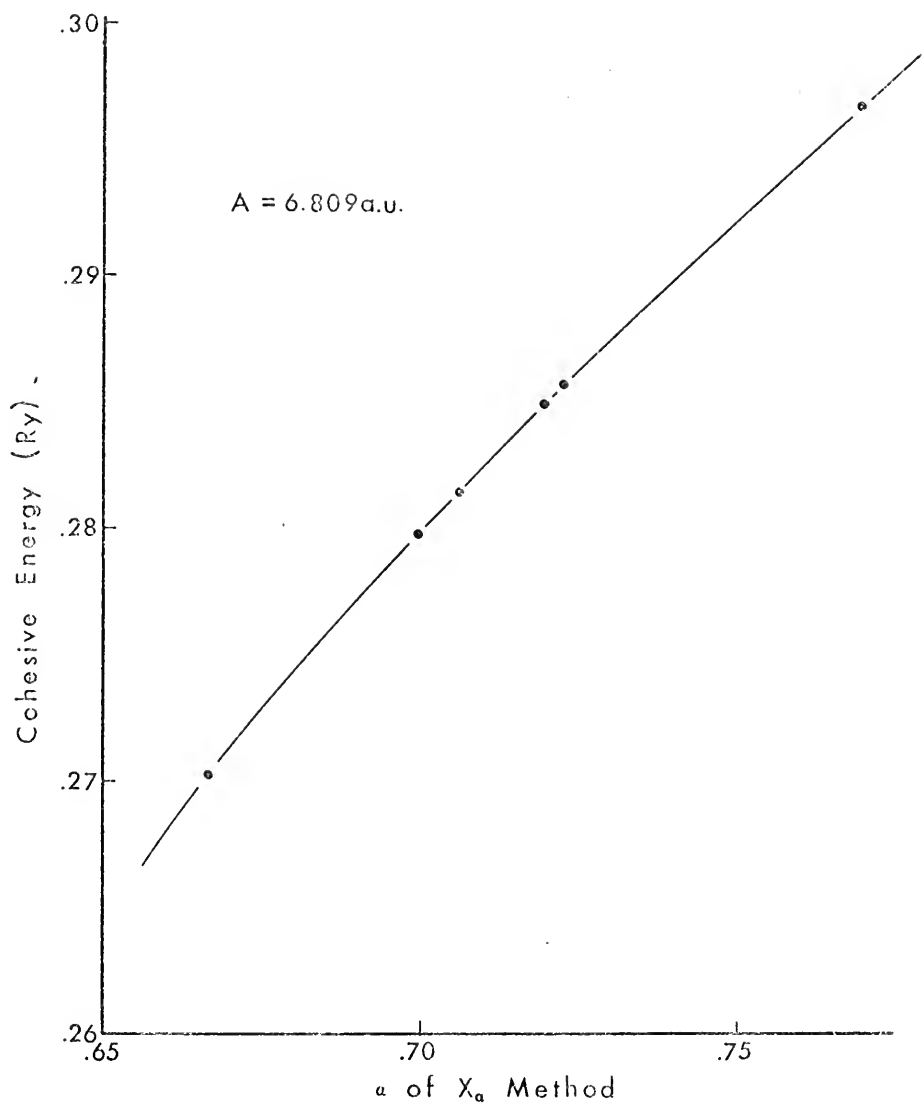


Figure C.7

dependence of total energy on α cannot be carried too far. Even so, the cohesive energy is a smooth function, increasing with increasing α .

If the cohesive energy curve given in Fig. C.7 is extended to intersect the experimental value of 0.257 Ry, the intersection will occur at a value of α somewhat below 0.64. This value of α would give Fermi surface "necks" too large in radius and a pressure at the experimentally determined lattice spacing of well over 100 Kb, both of which would be in very poor agreement with experimental results. This indicates that the $X\alpha$ method (using a single α , as in the present calculations) does not simultaneously give cohesive energy, pressure, and a Fermi surface that are in the best possible agreement with experiment. However, the calculated values of cohesive energy differ from the experimental value by less than 16% throughout this range of α . This is a small difference when we consider that the cohesive energies given in Table C.2 are the difference between two calculated energies, each of the order of 3200 Ry. It is quite possible, that increased precision in the present calculations could eliminate the large part of the differences between the calculated and experimentally determined cohesive energy.

LIST OF REFERENCES

1. J. C. Slater, Phys. Rev. 81, 385 (1951).
2. R. Gaspar, Acta Phys. Hung. 3, 263 (1954).
3. W. Kohn and L. J. Sham, Phys. Rev. 140, A1133 (1965).
4. Michael Boring and E. C. Snow, Phys. Rev. B 5, 1221 (1972).
5. E. C. Snow and J. T. Waber, Phys. Rev. 157, 570 (1967).
6. E. C. Snow, Phys. Rev. 171, 785 (1968).
7. E. C. Snow, Phys. Rev. 172, 708 (1968).
8. E. C. Snow, Phys. Rev. 158, 683 (1967).
9. M. Ross and K. W. Johnson, Phys. Rev. B 2, 4709 (1970).
10. J. C. Slater, Phys. Rev. 51, 846 (1937).
11. P. D. DeCicco, Doctoral Thesis, M.I.T. (1965).
12. F. Herman and S. Skillman, "Atomic Structure Calculations" (Prentice-Hall, Inc., Englewood Cliffs, New Jersey, 1963).
13. Terry Loucks, "Augmented Plane Wave Method" (W. R. Benjamin, Inc., New York, 1967).
14. L. F. Mattheiss, J. H. Wood, and A. C. Switendick, in "Methods in Computational Physics," edited by B. Alder, S. Fernbach, and M. Rotenberg (Academic Press, Inc., New York, 1968), Vol. 8, p. 63.
15. F. Seitz, "The Modern Theory of Solids," Ch. VIII (McGraw-Hill Book Company, Inc., New York, 1940).
16. J. W. D. Connolly, Doctoral Thesis, University of Florida (1966).
17. K. Schwarz, Phys. Rev. B 5, 2466 (1972).
18. I. Lindgren, Phys. Rev. Letters 19, 382 (1966); Arkiv Tysik 31, 59 (1966).

19. E. A. Kmetko, Phys. Rev. A 1, 37 (1970).
20. J. H. Wood, Intern. J. Quantum Chem. 35, 747 (1970).
21. M. Berrondo and O. Goscinski, Phys. Rev. 184, 10 (1969).
22. T. M. Wilson, J. H. Wood, and J. C. Slater, Phys. Rev. A 2, 620 (1970).
23. J. C. Slater, T. M. Wilson, and J. H. Wood, Phys. Rev. 179, 28 (1969).
24. J. C. Slater, "Advances in Quantum Chemistry," Vol. 6 (Academic Press, Inc., New York, 1972).
25. J. C. Slater and J. H. Wood, Intern. J. Quantum Chem. 4S, 3 (1971).
26. Frank W. Averill, Phys. Rev. B 4, 3315 (1971).
27. Frank W. Averill, University of Florida Quantum Theory Project Report No. 284 (1972).
28. T. M. Hattox, Doctoral Thesis, University of Florida (1972).
29. Frank W. Averill, Doctoral Thesis, University of Florida (1971).
30. P. O. Löwdin, Advan. Phys. 5, 1 (1956).
31. L. F. Mattheiss, Phys. Rev. 133, A1399 (1964).
32. J. C. Slater and P. DeCicco, M.I.T. Solid State and Molecular Theory Group Quarterly Progress Report, No. 50 (1963).
33. W. E. Rudge, Phys. Rev. 181, 1033 (1969).
34. C. Kittel, "Introduction to Solid State Physics" (John Wiley & Sons, Inc., New York, 1968).
35. Karl A. Gschneidner, Jr., in "Solid State Physics," Vol. 16, edited by F. Seitz and D. Turnbull (Academic Press, Inc., New York, 1964).

36. C. W. Berglund and W. E. Spicer, Phys. Rev. 136, A1044 (1964).
37. A. H. Lettington, Phys. Letters 9, 98 (1964).
38. D. E. Eastman and J. K. Cashion, Phys. Rev. Letters 24, 310 (1970).
39. I. Lindau and L. Wallden, Solid State Commun. 8, 1147 (1971).
40. J. F. Janak, A. R. Williams, and V. L. Moruzzi, Phys. Rev. B6, 4367 (1972).
41. B. Noumerov, Monthly Notices Roy. Astron. Soc. 84, 592 (1924).
42. P. C. Greisen, Phys. Status Solidi 25, 753 (1968).
43. D. R. Hartree, "The Calculation of Atomic Structures" (John Wiley & Sons, Inc., New York, 1957).
44. Charlotte Froese Fischer, Computer Phys. Com. 2, 124 (1971).
45. J. H. Wood, private communications.
46. B. Segal, Phys. Rev. 125, 109 (1962).
47. G. A. Burdick, Phys. Rev. 129, 138 (1963).
48. L. F. Mattheiss, Phys. Rev. 134, A970 (1964).
49. J. S. Faulkner, H. L. Davis, and H. W. Joy, Phys. Rev. 161, 656 (1967).
50. Shinya Wakoh, J. Phys. Soc. Japan 20, 1894 (1965).

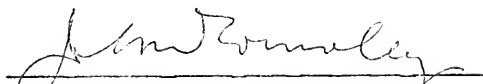
BIOGRAPHICAL SKETCH

Edward Clark Snow was born November 16, 1934, in University City, Missouri. He attended school in Litchfield, Illinois through his junior year of high school, and graduated from McAllen Senior High School in McAllen, Texas in June 1953. In January, 1954 he was inducted into the U. S. Army and received an honorable discharge from active duty in January, 1956. In January, 1958 he enrolled in Pan American College and received a Bachelor of Arts with majors in physics and mathematics in June, 1961. In September, 1961 he enrolled in the Graduate School of Texas A & M University as a National Defense Education Act, Title IV fellow, and received a Master of Science with a major in physics in January, 1965. In September, 1963 he became a staff member of the Los Alamos Scientific Laboratory in Los Alamos, New Mexico, where he has been employed since that time, with the exception of the period between May, 1964 and February, 1965, during which time he was employed with Esso Production Research in Houston, Texas.

He enrolled in the Graduate School of the University of Florida in September, 1968 on the Advanced Study Program provided by the Los Alamos Scientific Laboratory, and has been working toward the degree of Doctor of Philosophy since that time.


Edward Clark Snow is married to the former Patsy Ann Greenhill and has four children, Julianna, Sharilyn, Allison Ann, and Edward Clark, Jr. He is a member of Alpha Chi and a charter member of the Pan American College chapter of Sigma Pi Sigma.

I certify that I have read this study and that in my opinion it conforms to acceptable standards of scholarly presentation and is fully adequate, in scope and quality, as a dissertation for the degree of Doctor of Philosophy.



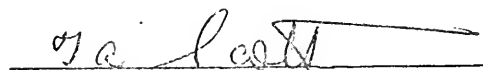
J. W. D. Connolly, Chairman
Associate Professor Physics

I certify that I have read this study and that in my opinion it conforms to acceptable standards of scholarly presentation and is fully adequate, in scope and quality, as a dissertation for the degree of Doctor of Philosophy.



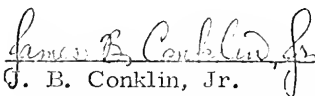
J. C. Slater
Graduate Research Professor of
Physics and Chemistry

I certify that I have read this study and that in my opinion it conforms to acceptable standards of scholarly presentation and is fully adequate, in scope and quality, as a dissertation for the degree of Doctor of Philosophy.



T. A. Scott
Professor of Physics

I certify that I have read this study and that in my opinion it conforms to acceptable standards of scholarly presentation and is fully adequate, in scope and quality, as a dissertation for the degree of Doctor of Philosophy.


J. B. Conklin, Jr.

Associate Professor of Physics

I certify that I have read this study and that in my opinion it conforms to acceptable standards of scholarly presentation and is fully adequate, in scope and quality, as a dissertation for the degree of Doctor of Philosophy.



C. E. Reid

Associate Professor of Chemistry

This dissertation was submitted to the Department of Physics and Astronomy in the College of Arts and Sciences and to the Graduate Council, and was accepted as partial fulfillment of the requirements for the degree of Doctor of Philosophy.

Dean, Graduate School

August, 1973

NM9 217.65 24

#399 Sec map. 113 (152)